Pharmacological Research 187 (2023) 106561

Contents lists available at ScienceDirect

Pharmacological Research

journal homepage: www.elsevier.com/locate/yphrs

1,5-disubstituted-1,2,3-triazoles counteract mitochondrial dysfunction acting on F_1F_O-ATPase in models of cardiovascular diseases

Cristina Algieri [a,1], Chiara Bernardini [a,1], Saverio Marchi [b,1], Maurizio Forte [c], Matteo Antonio Tallarida [d], Franca Bianchi [c], Debora La Mantia [a], Vincenzo Algieri [d], Rosita Stanzione [c], Maria Cotugno [c], Paola Costanzo [d], Fabiana Trombetti [a], Loredana Maiuolo [d,2], Monica Forni [a,e,2], Antonio De Nino [d,2], Flavio Di Nonno [c], Sebastiano Sciarretta [c,f], Massimo Volpe [g,h], Speranza Rubattu [c,g,2,3], Salvatore Nesci [a,3,*]

[a] Department of Veterinary Medical Sciences, University of Bologna, Ozzano Emilia 40064, Italy
[b] Department of Clinical and Molecular Sciences, Marche Polytechnic University, Ancona 60126, Italy
[c] IRCCS Neuromed, Pozzilli 86077, Italy
[d] Department of Chemistry and Chemical Technologies, University of Calabria, Cosenza 87036, Italy
[e] Health Sciences and Technologies-Interdepartmental Center for Industrial Research (CIRI-SDV), Alma Mater Studiorum-University of Bologna, Bologna 40126, Italy
[f] Department of Medical-Surgical Sciences and Biotechnologies, Sapienza University of Rome, Latina 04100, Italy
[g] Department of Clinical and Molecular Medicine, Sapienza University of Rome, Rome 00189, Italy
[h] IRCCS San Raffaele, Rome 00163, Italy

ARTICLE INFO

Keywords:
Mitochondria
Permeability transition pore
Triazoles
F_1F_O-ATPase
Cardiovascular diseases
Binding sites

ABSTRACT

The compromised viability and function of cardiovascular cells are rescued by small molecules of triazole derivatives (Tzs), identified as **3a** and **3b**, by preventing mitochondrial dysfunction. The oxidative phosphorylation improves the respiratory control rate in the presence of Tzs independently of the substrates that energize the mitochondria. The F_1F_O-ATPase, the main candidate in mitochondrial permeability transition pore (mPTP) formation, is the biological target of Tzs and hydrophilic F_1 domain of the enzyme is depicted as the binding region of Tzs. The protective effect of Tz molecules on isolated mitochondria was corroborated by immortalized cardiomyocytes results. Indeed, mPTP opening was attenuated in response to ionomycin. Consequently, increased mitochondrial roundness and reduction of both length and interconnections between mitochondria. In *in-vitro* and *ex-vivo* models of cardiovascular pathologies (*i.e.*, hypoxia-reoxygenation and hypertension) were used to evaluate the Tzs cardioprotective action. Key parameters of porcine aortic endothelial cells (pAECs) oxidative metabolism and cell viability were not affected by Tzs. However, in the presence of either 1 μM **3a** or 0.5 μM **3b** the impaired cell metabolism of pAECs injured by hypoxia-reoxygenation was restored to control respiratory profile. Moreover, endothelial cells isolated from SHRSP exposed to high-salt treatment rescued the Complex I activity and the endothelial capability to form vessel-like tubes and vascular function in presence of Tzs. As a result, the specific biochemical mechanism of Tzs to block Ca^{2+}-activated F_1F_O-ATPase protected cell viability and preserved the pAECs bioenergetic metabolism upon hypoxia-reoxygenation injury. Moreover, SHRSP improved vascular dysfunction in response to a high-salt treatment.

1. Introduction

Mitochondrial disorders are often linked to structural and morphological variations within cell caused by pathological conditions [1,2]. The main mitochondrial phenomenon responsible to trigger different forms of regulated cell death is loss of mitochondrial

* Corresponding author.
E-mail address: salvatore.nesci@unibo.it (S. Nesci).
[1] These authors contributed equally
[2] Senior authors
[3] Joint last authors.

https://doi.org/10.1016/j.phrs.2022.106561
Received 28 September 2022; Received in revised form 8 November 2022; Accepted 16 November 2022
Available online 21 November 2022

permeability transition (mPT). The biological event of mPT is mediated by the opening of a high conductance channel named mitochondrial permeability transition pore (mPTP) [3]. The F_1F_O-ATPase is a unique bifunctional enzyme in biology that support ATP synthesis/hydrolysis exploiting the feature of energy-transducing membranes of the chemiosmotic theory [4,5]. The F_O domain and the hydrophilic F_1 domain form F_1F_O-ATPase and these rotary motors are functionally and structurally coupled by a central rotor and a peripheral stator [6,7]. The F_O domain is a dissipator of the protonmotive force (Δp) through the inner mitochondrial membrane (IMM) by torque generation. The rotation drives the mechanical-power transmission of F_1 domain producing ATP with high kinetic efficiency [8]. The H^+-translocating F_1F_O-ATPase can also work in reverse to energize the IMM. In an energy-consuming process, the F_1 domain uses the free energy of ATP hydrolysis to power the F_O domain acting as an H^+ pump [9]. The mitochondria can undergo the mPT when Ca^{2+} concentration abruptly increases. Herein, Ca^{2+} binding to F_1F_O-ATPase can replace the natural cofactor Mg^{2+} bound in the catalytic sites into the F_1 domain by supporting ATP hydrolysis but not ATP synthesis of the enzyme [10]. According to the proposed "bent-pull-twist" model of *c*-subunit channel gating of mPTP opening [11], the monofunctional activity of Ca^{2+}-activated F_1F_O-ATPase hydrolyzes ATP and triggers the formation of the mPTP phenomenon [12,13].

Triazole derivatives (Tzs) are small molecules currently known as novel potent inhibitors of the mPTP [14,15]. Tzs are obtained by replacing the isoxazole with triazole core in analogue compounds. Tzs used in the present work (**3a** and **3b**) are obtained *via* eliminative azide–olefin cycloaddition reaction, starting from arylnitroolefins **1** as dipolarophile, benzylazide **2** as dipole and a Lewis Acid/Ionic Liquid system as an eco-sustainable catalyst (Scheme 1) [16,17].

Tz structural portion enhances the chemical interactions with the mitochondrial target(s). Furthermore, the presence of substituents allows forming of interactions with the biomolecules [18]. In addition, the further insertion of functional groups will allow the realization of di- and trisubstituted Tzs with particular structural geometry that will make more selective their ability to interact with the biological target [19]. Structure-activity relationship optimization studies around the 1,2,3-triazole scaffold have highlighted that only F_1F_O-ATPase activity sustained by Ca^{2+} can be selectively inhibited with either **3a** (1-Benzyl-5--phenyl-1,2,3-triazole) or **3b** (1-Benzyl-5-(2-nitrophenyl)– 1,2,3-triazole) compounds [14].

Ca^{2+}-activated F_1F_O-ATPase is the lethal functional mode of the mitochondrial enzyme that triggers mPTP. The promising *in vitro* pharmacological profile of bioactive Tzs counteracts the mPTP formation [20]. Medical chemistry insights can address drug design to target the F_1F_O-ATPase in human pathologies in which dysfunction of mtPTP plays a key role [21]. Cardiovascular diseases (CVDs) are sustained by mitochondrial dysfunction and the risk of deleterious cardiovascular events increases when mPTP forms. Moreover, F_1F_O-ATPase can confer a molecular mechanism of cardioprotection to myocardial ischemia blocking mPTP formation by protein dephosphorylation linked to G protein-coupled receptor signalling [22,23]. Remarkable protection in heart injury induced by ischemia-reperfusion is influenced by mPTP desensitization. The first attempt to inhibit mPTP by targeting the *c* subunits of the membrane F_O domain using small molecules has provided relevant therapeutic insights into reperfusion injury in myocardial infarction [24].

Specifically, mPTP inhibition by Tzs and the identification of the binding region on Ca^{2+}-activated F_1F_O-ATPase might corroborate the link between the mPTP phenomenon and the enzyme. Our studies aimed to endorse the protective effect of Tzs on impaired mitochondria in different contexts starting from the molecular mechanism of mPTP formation in mitochondria and cardiomyocytes to *in vitro* and ex *vivo* models of cardiovascular pathologies (hypoxia-reoxygenation and hypertension). Event of hypoxia-reoxygenation and hypertension condition promoting stroke were studied on porcine Aorta Endothelial Cells (pAECs) line and cerebral Endothelial Cells (ECs) of Spontaneously Hypertensive Stroke Prone Rat (SHRSP), respectively. In both models, cell death would lead to the phenomenon of mPTP formation. Overall, our work shows that specific biochemical mechanism of Tzs to block the mPTP on isolated mitochondria and cardiomyocytes versatility counteracts the post-ischemic reperfusion injury and hypertension-related vascular damage.

2. Materials and methods

2.1. Preparation of the mitochondrial fraction

Swine hearts were collected in a local abattoir and transported to the laboratory within 2 h at 0–4 °C. After removing the fat and blood clots, approximately 30–40 g of heart tissue was rinsed in ice-cold Tris-HCl wash buffer (medium A) consisting of 0.25 M sucrose, 10 mM Tris (hydroxymethyl) - aminomethane (Tris), pH 7.4, and chopped into fine pieces with scissors. Once rinsed, the tissues were gently dried on absorbent paper, weighed and homogenized in a buffer (medium B) consisting of 0.25 M sucrose, 10 mM Tris, 1 mM EDTA (free acid), 0.5 mg/mL BSA and pH 7.4 with HCl in a ratio of 10 mL medium B per 1 g of fresh tissue. After a delicate preliminary break by Ultra-Turrax® T25 to 8000 r/min to fragment the heart's fibrous tissue and then the fabric was carefully homogenized by a motorized Teflon pestle homogenizer (Braun Melsungen type 853202) at 650 rpm with three strokes up and down. Subsequently the mitochondrial fraction was obtained by gradual centrifugation as detailed in Nesci et al. [25].

2.2. F_1 domain purification

After thawing, the mitochondrial suspensions of the swine heart were diluted with 50 mL of medium A to obtain a concentration of 20 mg/mL of protein, sonicated on ice with Sonicator MSE Soniprep 150 to an amplitude of 210 μm by 3. minutes three times with 30 s intervals and centrifuged at 10,000 ×*g* for 10 min. The supernatant from this first centrifugation was further centrifuged at 100,000 ×*g* for 2 h. All these centrifugation steps were performed at 4 °C. The pellet was resuspended in medium A plus 4 mM Na_2ATP, the pH was adjusted to 9.2 by adding small aliquots of 20% (w/w) NH_4OH solution and stored overnight at 4 °C. The next day, the suspension, in which the pH was brought back to

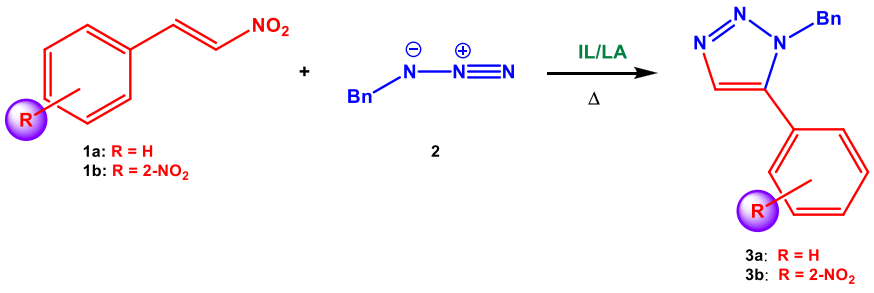

Scheme 1. Synthetic approach to the formation of Tzs **3a** and **3b**.

8.0 by adding small aliquots of aqueous solution of 2 N HCl, was sonicated at an amplitude of 210 μm for 5 min and then centrifuged at 300,000 ×*g* for 1 h [26]. The resulting pellet was resuspended in 9 mL of medium A plus 2 mM EDTA, pH 7.6. After the addition of 4.5 mL of chloroform, the resulting mixture was vigorously vortexed for 15 s and centrifuged at 600 ×*g* for 10 min to allow for separation of the two phases. The upper aqueous phase was collected and further centrifuged at 100,000 ×*g* for 1 h. The obtained pale yellow supernatant was supplemented with adequate aliquots of freshly prepared ATP solution to obtain a final 4 mM ATP concentration and with a 2 N NaOH solution to adjust pH to 8.0. After the dropwise addition of saturated solution $(NH_4)_2SO_4$ plus 5 mM EDTA under continuous stirring to obtain a saturation of 37% and a pH adjustment to 8.0 with a 1 N KOH solution [26], the suspension was centrifuged at 10,000 ×*g* for 15 min. Pellet was discarded and the collected supernatant was brought to 60% saturation with solid $(NH_4)_2SO_4$; the mixture was then adjusted to pH 8.0 with a 1 N solution of KOH and kept overnight at 4 °C [26]. Finally, pellet from the last centrifugation at 150,000 ×*g* for 90 min, was resuspended by gentle homogenization using a Potter Elvehjem Teflon homogenizer in a small volume of medium containing 100 mM Tris/H_2SO_4, 1 mM EDTA and 50% glycerol, pH 8.0, constituted the partially purified F_1 fraction [13,26]. Protein concentration was determined according to the Bradford colourimetric method by Bio-Rad Protein Assay kit II using BSA as standard [27]. Once it was verified that in the partially purified F_1 fraction, ATPase activity, supported by Ca^{2+} or Mg^{2+}, was completely insensitive to 1 μg/mL of oligomycin, thus demonstrating the detachment of the F_O sector, the partially purified F_1 fraction was then preserved in liquid nitrogen and no further purification was carried out.

2.3. F-ATPase activity assay

Immediately after thawing, the mitochondrial preparations were used for the F-ATPase activity assays. The capacity of ATP hydrolysis was evaluated in a reaction medium (1 mL) containing 0.15 mg of mitochondrial protein and ethanolamine-HCl buffer 75 mM pH 9.0, Na_2ATP 6.0 mM and $MgCl_2$ 2.0 mM for Mg^{2+}-activated F_1F_O-ATPase assay and a buffer test itself at pH 8.8 plus 3.0 mM Na_2ATP and 2.0 mM $CaCl_2$ for Ca^{2+}-activated F_1F_O-ATPase assay as detailed in Nesci et al. [28].

2.4. F_1-ATPase activity assay

Immediately after thawing, partially purified F_1 domains were used for F_1-ATPase activity assays. The capability of ATP hydrolysis was assayed in a reaction medium (1 mL) containing 0.15 mg F_1 purified protein and 75 mM ethanolammine–HCl buffer pH 9.0, 6.0 mM Na_2ATP, and 2.0 mM $MgCl_2$ or 2.0 mM $CaCl_2$ for Mg^{2+}-activated F_1F_O-ATPase and Ca^{2+}-activated F_1F_O-ATPase assays, respectively. The methods and parameters of ATP hydrolysis and Pi detection were the same as those used for the mitochondrial F-ATPase activity assays. The sensitivity to 1 μg/mL oligomycin was tested to verify the detachment of F_O domain [13].

2.5. SDS-PAGE and western blot assay

For SDS-PAGE assay, aliquots containing 5 μg of partially purified F_1 domain proteins were separated on BoltTM 4–12% bis-Tris Plus (Life Technologies Ltd., Paisley, UK) for 55 min at 165 volts. At the end of the electrophoresis, the gel was washed three times at room temperature with deionized water for 5 min with each wash. The gels were then stained with SAFE BLUE (Coomassie blue) for 1 h with gentle agitation and bleached according to manufacturer's instructions.

For the western blot test, proteins separated from SDS-PAGE were electrophoretically transferred onto a nitrocellulose membrane using the semi-dry TurboTM Blot System (Bio-Rad Laboratories Inc., Berkeley, CA). The stain was washed in PBS and the protein transfer was checked by staining the nitrocellulose membranes with 0.2% Ponceau Red. Non-specific binding on nitrocellulose membranes was blocked with 5% milk powder in PBS-T20 (phosphate buffered saline + 0.1% Tween-20) for 1 h at room temperature. The membrane was then incubated overnight at 4 °C with a 1:1000 dilution of anti-ATP5B rabbit polyclonal antibody (Aviva Systems Biology) in PBS-T20. After several washes with PBS-T20, the membrane was incubated with the biotin-conjugated secondary antibody (goat anti-rabbit IgG antibody) and then with a 1:1000 dilution of an anti-biotin horseradish peroxidase-bound antibody. Western blots were developed using a chemiluminescent substrate (Clarity Western ECL Substrate) according to the manufacturer's instructions. The chemiluminescent signal intensity of the resulting bands was acquired by a Fluor-ST MultImager using Quantity One software (Bio-Rad Laboratories Inc.).

2.6. Kinetic analysis

Kinetic studies have been conducted on the mutual exclusion of different inhibitors on the same F-ATPase activity. These analyzes aimed to shed light on the possible interaction on the F_1 domain between compounds **3a** and **3b** and resveratrol or NBD, between **3b** and tetranitromethane between **3a** and azide. To build Dixon-like graphs, in which reciprocal data on enzymatic activity (1/v) (*y*-axis) *versus* resveratrol, NBD, tetranitromethane and azide (*x*-axis) concentration, F-ATPase activity were plotted was analyzed without and with specific concentration of **3a** and **3b** and at constant concentration of ATP substrate. According to the graphical method [29] employed, when the straight lines show different slopes and intersection points, the enzyme inhibition mirrors the combined effect of two inhibitors. When F-ATPase is inhibited by two non-mutually exclusive compounds, for example **3a** or **3b** (I_1) plus F_1 inhibitor (I_2), the enzyme can combine with both inhibitors to produce the EI_1I_2 [30] quaternary complex. The value of $-\alpha K'_i$, which represents the dissociation constant of the quaternary complex EI_1I_2, was calculated from the abscissa (changed to positive) of the intersection point of the two lines obtained in the presence and absence of F_1 inhibitor. The interaction constant α was then calculated from the ratio between $\alpha K'_i$ and K'_i.

2.7. Docking studies

The study was performed using the crystal structures of ATP synthase retrieved from the Protein Data Bank (http://www.rcsb.org/). Molecular docking was performed with AutoDock Vina, [31] bykepting the docking parameters at default values. The geometries of **3a** and **3b** were previously optimized using quantum mechanics. Geometry optimizations and frequency calculations for stationary point characterization were carried out with Gaussian16 using the M06–2X hybrid functional [32], the 6–31 G(d,p) basis set, and ultrafine integration grids. Bulk solvent effects in water were considered implicitly through the IEF-PCM polarizable continuum model [33]. The protein structures were processed with AutodockTools-1.5.6rc3 [34] to toggle problems of incomplete structures due to missing atoms or water molecules. Ligand and protein structure files were converted to PDBQT (Protein Data Bank Partial Charge and Atom Type) and the docking was executed using the Lamarckian algorithm. A grid box was then constructed to define docking spaces.The position of the grid box was set on the plausible site of interaction of the Tzs, which for **3a** was the active site of the enzyme without the azide inhibitor (PDB code: 2CK3), and for **3b** the interacting site of NBD-Cl (PDB code: 1NBM). The grid box consisted of 25 grid points in all three dimensions (X, Y, and Z) separated by a distance of 1 Å between each one. The docking protocol was also validated by simulating the pose of resveratrol (RES) in the crystal structure (PDB code: 2JIZ), obtaining a low discrepancy between the pose of the docked ligand and the pose of the crystallographic ligand. The crystallographic ligand was docked after adding hydrogen atoms with AutodockTools-1.5.6rc3 [34] and without optimizing its geometry. For

all the simulations, the protein was kept rigid.

2.8. Oxidative phosphorylation assay

Respiratory activity on freshly isolated mitochondria was evaluated polarographically by a Clark-type electrode using a thermostatted Oxytherm system (Hansatech Instruments, King's Lynn, United Kingdom) in terms of oxygen consumption at 37 °C in a 1 mL polarographic chamber. The reaction mixture, kept at a fixed temperature and continuously stirred, contained 0.25 mg/mL mitochondrial suspension, 40 mM KCl, 0.2 mg/mL fatty acid-free BSA, 75 mM sucrose, 0.5 mM EDTA, 30 mM Tris–HCl, pH 7.4 and 5 mM KH_2PO_4, plus 3 mM $MgCl_2$. The reaction was carried out at a fixed temperature and under constant stirring. The assessment of the rate of oxygen consumption was carried out in the presence of specific substrates. Concerning complex I, the substrates were glutamate/malate in a ratio of 1:1; for complex II, the substrate was succinate. Furthermore, complex I was inhibited by 1 μg/mL of rotenone, while inhibition of complex III was obtained by 1 μM of antimycin A. The oxidation of glutamate/malate allowed to determine NADH ubiquinone oxidoreductase activity, on the other hand, oxidation of succinate represented the multicomponent pathway of succinoxidase, *i.e.* the flow of electrons in respiratory chain through complex II. By adding 1 μM of antimycin A to the respective tests with glutamate/malate and succinate, it was possible to evaluate the non-specific oxygen consumption. To evaluate the coupling between respiratory activity and phosphorylation, 150 nmol of ADP at state 2 of respiratory mitochondria was added [35]. The respiratory control ratio (RCR) of OXPHOS was evaluated as the ratio of state 3 (when ATP is synthesized) to state 4 (when ATP is not synthesized). To evaluate the effects of compounds **3a** and **3b**, mitochondrial suspensions were added simultaneously with 1.0 μM and 0.5 μM of solution of **3a** or **3b**, respectively to the polarographic chamber before starting the reaction at 37 °C. Respiratory activities were expressed as nmoles of protein $O_2 \bullet mg^{-1} \bullet min^{-1}$. The experimental protocol involved the injection (in a very precise order) of reagents into the polarographic cell using a syringe. In particular, to the mitochondrial protein suspensions, in the presence and absence of compounds **3a** and **3b**, the following were added: inhibitors of the previous passages of the respiratory chain (when required), substrate (s), ADP, and inhibitors (rotenone for glutamate/malate-stimulated and antimycin A for succinate-stimulated respiration). The rate of oxygen consumption was evaluated in the presence of the specific substrates, glutamate/malate for complex I and succinate for complex II. Polarographic assays were performed at least in triplicate.

2.9. mPTP and membrane potential evaluation in mitochondria

Swine heart mitochondria (1 mg/mL) were suspended and energized in assay buffer (130 mM KCl, 1 mM KH_2PO_4, 20 mM HEPES, pH 7.2 with Tris) incubated at 37 °C with 1 μg/mL of rotenone and 5 mM succinate as a respiratory substrate. The opening of mPTP was induced by the addition of low concentrations of Ca^{2+} (20 μM) at fixed time intervals (1 min). Calcium retention capacity (CRC) was evaluated spectrofluorophotometrically in the presence of 0.8 μM of Fura-FF. The probe has different spectral properties in the absence and presence of Ca^{2+}, *i.e.* it shows excitation/emission spectra of 365/514 nm in the absence of calcium (Fura-FF low Ca^{2+}) and moves to 339/507 nm in the presence of calcium concentrations (Fura-FF high Ca^{2+}). PTP opening, implying a decrease in CRC, was detected by increasing the fluorescence intensity ratio (Fura-FF high Ca^{2+})/(Fura-FF low Ca^{2+}). Membrane potential (Δφ) was evaluated in the presence of 0.5 μM JC-10. In polarized mitochondrial membranes, this probe selectively generates an orange JC-10 aggregate (excitation/emission spectra of 540/590 nm). The JC-10 monomers, generated when Δφ decreases, cause a green shift (excitation/emission spectra of 490/525 nm). Consequently, membrane depolarization (decrease in Δφ) attributed to mPTP formation was detected by the increase in the fluorescence intensity ratio, which corresponds to an increase in the aggregate JC-10/monomers JC-10 ratio [13]. All measurements were processed by LabSolutions RF software.

2.10. Mitochondrial membrane potential measurements in cells

For experiments in intact AC16 cells, mitochondrial membrane potential was measured by loading cells with 100 nM tetramethyl rhodamine methyl ester (TMRM) for 30 min at 37 °C and then imaged over time using a 3D Cell Explorer-fluo microscope (Nanolive, Switzerland) as previously described [36]. Basal levels were normalized on fluorescence in presence of FCCP (carbonyl cyanide ptrifluoromethoxyphenylhydrazone, 10 μM), a strong uncoupler of oxidative phosphorylation.

2.11. Quantitative evaluation of nitrotyrosine and dityrosine

The possible formation of nitrotyrosine and dithyrosine in the presence of compound **3b** as a post-translational modification was evaluated spectrophotometrically [37]. Increasing amounts of compound **3b** (0 – 0.5 – 1.0 and 2.0 μmol) were added in medium A to 300 μg of mitochondrial suspensions and incubated for 30 min at room temperature. In each series of experiments, the same volume of medium A without compound **3b** was added in parallel with the sample in the absence of Tz used as controls. Then, aliquots of pre-incubated mitochondrial suspensions were added to 75 mM ethanolamine-HCl buffer, pH 11.0 to produce a final volume of 2.0 mL in the quartz cuvette. After 1 min of acclimatization at 37 °C under magnetic stirring, the absorbance was read on the spectrophotometer. On the same sample, automatically by changing the absorption wavelength, the nitrotyrosine content was evaluated by detecting the absorbance at 430 nm, while the formation of dithyrosine was calculated from the increase in absorbance at 330 nm. In each experimental set, according to the Lambert-Beer law, the absorbance values were converted into concentration values using the nanomolar extinction coefficients (ε) of nitrotyrosine ($\varepsilon_{430\ nm}$= 4400 M^{-1} cm^{-1}) and dithyrosine ($\varepsilon_{330\ nm}$= 4000 M^{-1} cm^{-1}), respectively. All data were expressed as nmol nitrotyrosine or dithyrosine/μg mitochondrial protein [25].

2.12. Cell culturee

AC16 human cardiomyocyte cell line was grown in DMEM/F12 containing 2 mM L-glutamine, 12.5% FBS and 1x PS solution. Cells were only used up to passage 10.

Primary cell cultures of pAECs were isolated and maintained as previously described [38]. All experiments were performed using pAECs between passages 3–8. The cells were seeded and routinely cultured in T25 or T75 primary culture flasks (2×10^4 cells/cm^2) in a human endothelial serum-free medium (hESFM) with 5% FBS and 1 ×antibiotic/antimycotic solution in a 5% CO_2 atmosphere and 38.5 °C.

Cerebral ECs were isolated from brains of neonatal (days 1–3) SHRSP using mechanic and enzymatic digestions followed by a CD31 + magnetic positive selection (Miltenyi Biotec, Bergisch Gladbach, Germany). ECs were cultured as previously reported [39]. Cells between passages 1–4 were used for all experiments.

2.13. Mitochondrial morphology analysis

AC16 cells, grown onto 13-mm coverslips were washed with PBS and fixed in 4% formaldehyde for 10 min at room temperature. After washing three times with PBS, cells were permeabilized with 0.1% Triton X-100 in PBS (PBS-T) for 10 min at room temperature and then blocked with PBS-T containing 5% BSA at room temperature for 1 h. Cells were then incubated with TOMM20 primary antibodies (Cat # HPA011562; RRID:AB_1080326), overnight at 4 °C, to detect the

mitochondrial network. Then, cells were washed 3 times with PBS-T, and incubated with the appropriate isotype matched, AlexaFluor-conjugated secondary antibodies. Coverslips were mounted with ProLong Gold Antifade reagent (Thermo Fisher Scientific) at room temperature, and images were acquired with confocal microscope (Zeiss LSM510) using a 63 × 1.4 NA Plan-Apochromat oil-immersion objective. The analysis were conducted using the plugin "Mitochondria Analyzer" [40,41], available on Fiji.

2.14. Calcein-cobalt quenching assay

AC16 cells were seeded onto 24-mm glass coverslips and the day after were loaded with calcein loading solution (1 mM calcein acetoxymethyl ester, 2 mM Co^{2+}, and sulfinpyrazone 200 μM) for 15 min at 37 °C in a 5% CO_2 atmosphere [42]. Cells were washed three times and image acquisition was performed with 3D Cell Explorer-fluo microscope (Nanolive, Switzerland). The mPTP activity was measured as the drop in calcein fluorescence before and after 10 min of 1 μM ionomycin.

2.15. Cell death assay

AC16 cell death was quantified using a Tecan Infinite 200 Pro microplate reader. Cell death assays were performed in medium w/o HCO_3^- supplemented with 2% FBS. Ac16 cells were seeded at the same number (5000 cells x well) on 96 well black/clear bottom plates, loaded with the cell impermeable dye SYTOX™ Green Nucleic Acid Stain (final concentration: 1 μM) and treated for 1 h with 1 μM ionomycin or 250 μM H_2O_2.

2.16. In vitro hypoxia/reoxygenation

To analyse the effect of the 3a and 3b on cell viability, pAECs were seeded in 96-well plates at a density of 1×10^4 cells/well, and, the day after, were exposed to increasing doses of **3a** and **3b** (0.1, 0.5, 1, 5, 10, 20, 30, 40, 50 μM) for 1 h.

The protective effect of the Tzs: **3a** and **3b** (0.1, 0.5, 1 μM) was assayed by a model of *in vitro* hypoxia/reoxygenation on pAECs: pAECs culture medium was replaced by an acid buffer (137 mM NaCl, 12 mM KCl, 0.9 mM $CaCl_2$, 0.49 mM $MgCl_2$, 4 mM HEPES and 20 mM sodium DL-lactate at pH 6.2) then cells were placed in a modular incubator chamber (Billups-Rothenberg USA) containing a gas mixture (1% O_2, 5% CO_2 and 94% N_2) for 13 h, after that, the normoxic conditions and the complete culture medium were restored for 24 h (reoxygenation) before the cell viability assay and cell metabolism analysis. Control group (CTR) was represented by pAECs cultured in normoxic conditions and in cell culture medium with vehicle DMSO (0.01%).

2.17. Cell viability

To analyse the effect of the 3a and 3b on cell viability, pAECs were seeded in 96-well plates at a density of 1×10^4 cells/well, and, the day after, were exposed to increasing doses of **3a** and **3b** (0.1, 0.5, 1, 5, 10, 20, 30, 40, 50 μM) for 1 h. ECs were treated with 20 mM NaCl for 72 h either in the presence or in the absence of **3a** (1 μM) or **3b** (0.5 μM).

Cell viability in treated pAECs or ECs was evaluated by 3-(4,5-dimethylthiazol-2-yl)− 2,5-diphenyltetrazolium bromide (MTT) assay (Sigma Aldrich, M5655) as previously described (Algieri et al., 2022) Briefly, MTT substrate was added to the culture medium for 3 h after that the MTT solubilization solution was added to dissolve the formazan crystals. The formazan absorbance was measured at a wavelength of 570 nm, using Infinite® F50/Robotic absorbance microplate readers from TECAN (Life Sciences). The background absorbance of multiwell plates at 690 nm was also measured and subtracted from the 570 nm measurements.

2.18. Cell metabolism

Using Seahorse XFp analyzer (Agilent, USA), oxygen consumption rate (OCR), cellular respiration index (pmol/min) and the extracellular acidification rate (ECAR), glycolysis index (mpH/min) were measured.

pAECs (20×10^3/well) were cultured in XFp cell culture mini-plates (Agilent, USA) for 24 h. On the day of the experiment, the cells were switched to a freshly made DMEM Seahorse XF medium of pH 7.4 supplemented with 10 mM glucose, 1 mM sodium pyruvate and 2 mM L-glutamine. The analyzes were carried out in the absence (control) and in the presence of 0.5 μM and 1 μM of both compounds **3a** and **3b** for the ATP Rate Assay and for the Cell Mito Stress Test using kits form Agilent. In the I/R model, 1 μM of compound **3a** and 0.5 μM compound **3b** for the Mito Stress Test was evaluated. OCR and ECAR were measured with the ATP Rate Assay and Cell Mito Stress Test programs after the plates were incubated for 45 min at 37 °C in air. In addition, the injection ports of XFp sensor cartridges were hydrated overnight with the XF calibrant at 37 °C; they were subsequently loaded with 10 times the concentration of inhibitors, as indicated by the instructions for the Seahorse XFp ATP Rate assay Test and the Cell Mito Stress Tes. Final concentrations of 1.5 μM oligomycin (port A) and 0.5 μM rotenone (Rot) plus 0.5 μM antimycin A (AA) (port B) were used for the ATP Rate Assay. Instead, for the Cell Mito Stress Test, the final concentrations were 1.5 μM oligomycin (olig) (port A), 1.0 μM carbonyl cyanide-4-(trifluoromethoxy) phenylhydrazone (FCCP) (port B) and 0.5 μM of rotenone plus antifungal A (port C) [43].

The ATP Rate Assay allows deriving bioenergetic parameters used to characterize the cellular production of ATP, *i.e.* the speed of ATP production, correlated to the conversion of glucose into lactate in the glycolytic pathway (glycoATP production rate) and to mitochondrial OXPHOS (production rate of mitoATP). Consequently, the ratio of mitoATP production rate to glycoATP production rate (ATP rate index) is currently considered a valuable parameter for detecting changes and differences in metabolic phenotype (a ratio > 1 means primarily *via* OXPHOS; ratio < 1 mainly means glycolytic pathway).

The Mito Stress Test allows obtaining the following parameters on mitochondrial respiration: basal respiration (basic OCR before the addition of oligomycin); minimal breathing (OCR in the presence of oligomycin); maximum respiration (OCR after the addition of FCCP). The so-called proton escape (difference between basal respiration and respiration in the presence of oligomycin or minimal respiration) indicates the re-entry of H^+ into the intermembrane space independently of ATP synthase. Non-mitochondrial respiration, assessed as OCR in the presence of rotenone plus antimycin A (respiratory chain inhibitors), was subtracted from all the above parameters. Turnover of ATP, or oligomycin-sensitive respiration, was obtained from the difference between basal respiration and minimal respiration (OCR in the presence of oligomycin). Finally, the difference between maximal and basal respiration provided reserve capacity, which represents the ability to respond to increased energy demand and can be considered a measure of the flexibility of OxPhos machinery.

2.19. NAD:NADH ratio

NAD^+ and NADH levels were measured in SHRSP ECs by using commercially available colorimetric kits (Abcam ab65348). NAD^+ and NADH values were read at 450 nM by a microplate reader and NAD^+: NADH ratio was calculated as reported by the manufacturer's protocol.

2.20. In vitro angiogenesis assay

Angiogenesis was performed by Matrigel assay. Briefly, Matrigel matrix growth factor reduced (BD Biosciences) was seeded in a 96 multiwell and allowed to solidify for 1 h at 37 °C. 1×10^4 ECs collected after each specific treatment were seeded on top of the Matrigel layer and incubated for 5 h. Images were taken with an optical inverted

microscope (Zeiss, Jena, Germany) fitted with a digital camera, and the number of master junctions was quantified using ImageJ software (National Institutes of Health, Bethesda, MD) and Image J plugin Angiogenesis analyzer.

2.21. Vascular reactivity experiments

Male SHRSP were fed with JD as previously reported for 4 weeks. At the end of the treatment, rats were sacrificed and mesenteric arteries were isolated. To perform the vascular reactivity experiments, the mesenteric arteries were placed in a pressure myograph system filled with Krebs solution. Vasorelaxation was assessed by measuring the dilatory responses of mesenteric arteries to cumulative concentrations of acetylcholine (from 10^{-9} M to 10^{-5} M) in vessels precontracted with phenylephrine as previously described [44]. Responses were assessed after incubation with or without **3a** (1 μM) or **3b** (0.5 μM) treatment for 1 h. All studies involving animals were performed in accordance with the Italian and European Community (Directive 2010/63/EU) for animal experiments, and the protocol was approved by IRCCS Neuromed OPBA (Organismo Preposto al Benessere Animale) and by the Italian Ministry of Health (authorization n. 1086/2020).

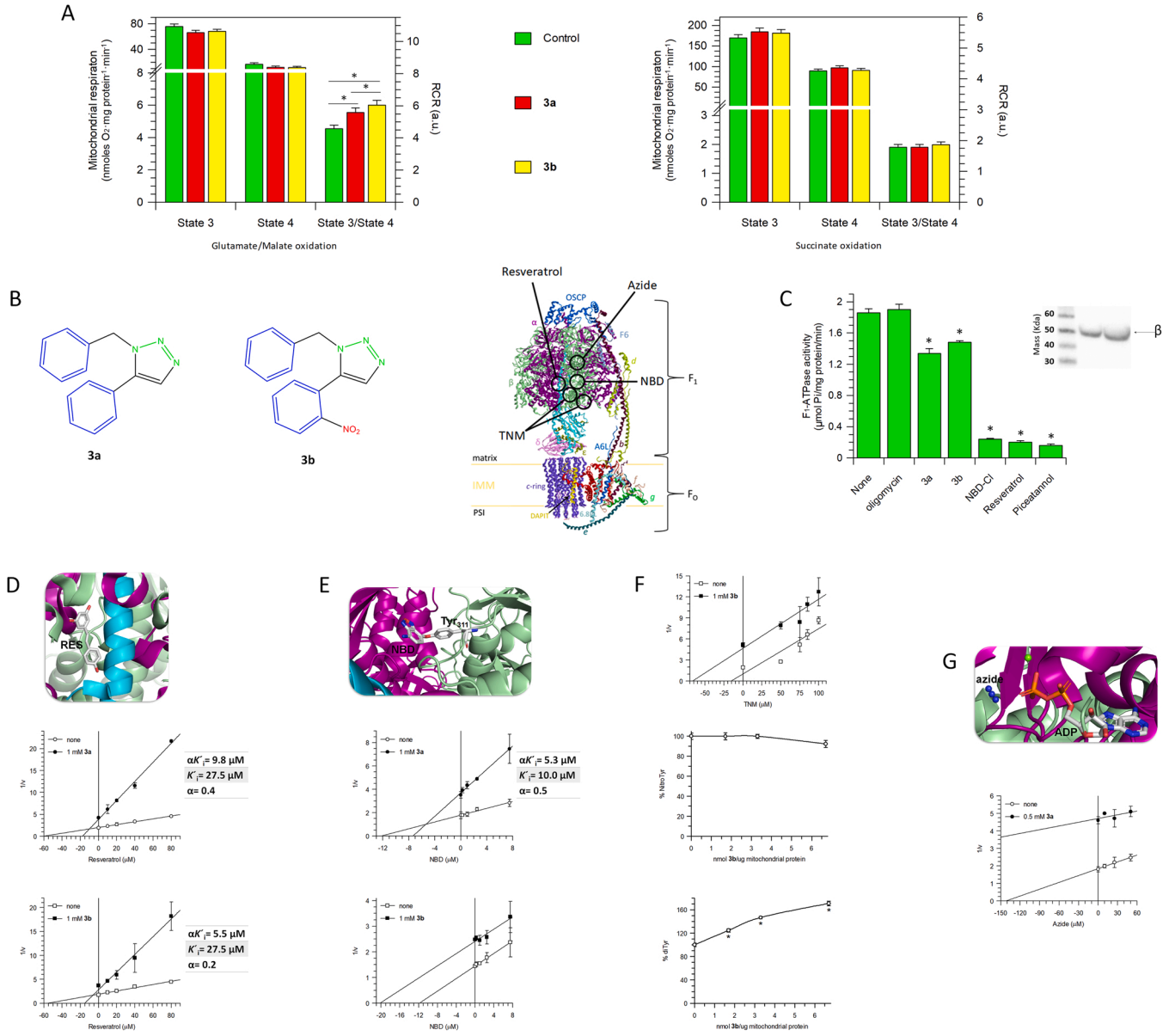

Fig. 1. Mitochondrial sensitivity to the 3a and **3b** Tz derivatives and druggable structures. A) Tzs effects on selected oxidative phosphorylation parameters: state 3 and 4 respiration and their ratio. Glutamate/malate- and Succinate-stimulated mitochondrial respiration in the absence and in the presence of 1.0 mM **3a** and 0.5 mM **3b**. B) Chemical structures of the compounds **3a** and **3b** and structure of the mammalian mitochondrial F_1F_O-ATPase have been obtained by ChemDraw and Chem3D software, respectively. The enzyme subunit composition is drawn as ribbon representations obtained from modified PDB ID code: 6TT7. The letter colours are the same as those of the subunits to which the structures belong. C) F_1-ATPase activity was evaluated in the absence or presence of the inhibitors: 3 μg/mL oligomycin; 1.0 mM **3a**, 0.5 mM **3b**, 75 μM NBD-Cl, 0.8 mM resveratrol, and 0.2 mM piceatannol. On the right hand, the β subunit band was identified by western blot assay. F_1 structure bound to resveratrol (RES) (D) or NBD (E) and multiple inhibitor analysis by Dixon plots for the **3a** and **3b** compounds. F) Mutual exclusion test **3b** and TNM evaluation of tyrosine post-translational modifications by the formation of nitrotyrosine or dityrosine. G) Azide bound to the F_1 domain and inhibition analysis of azide and **3a** mutually exclusive. RES, NBD, Tyr-311, azide, and ADP are illustrated as a ball-and-stick model. The data expressed as column charts (A,C) or points (D,E,F,G) represent the mean±SD (vertical bars) from at least three experiments carried out on different mitochondrial preparations. * indicates significant differences from control (none) at $P \leq 0.05$.

2.22. Statistical analysis

Statistical analyses were performed by SIGMASTAT software. Each treatment was replicated three or eight times (viability test) in three independent experiments. The data were analyzed by the Student's *t* test or by one-way analysis of variance (ANOVA) followed by Students–Newman–Keuls' test when *F* values indicated significance ($P \leq 0.05$) was applied. The analysis of variance followed by Students–Newman–Keuls' test when *F* values indicated significance ($P \leq 0.05$) was applied. Percentage data were *arcsin*-transformed before statistical analyzes to ensure normality.

3. Results

3.1. The effect of 3a and 3b compounds on oxidative phosphorylation and the interaction with the F_1 portion of Ca^{2+}-activated F_1F_O-ATPase

To validate the protective effect of Tzs on mPTP opening corroborated by the absence of negative effects on the mitochondrial bioenergetics, oxidative phosphorylation (OXPHOS) was evaluated in the presence of glutamate/malate or succinate as substrates for the Complex I (C-I) or Complex II (C-II), respectively. State 3 respiring (ADP-stimulated) mitochondria and State 4, obtained when added ADP is phosphorylated maximally to ATP in State 3, were unaffected by Tzs independently of the substrate to the C-I or C-II. However, only the coupling between glutamate/malate oxidation and ADP phosphorylation, evaluated as the state 3/state 4 ratio, was improved by Tzs. Regarding the glutamate/malate oxidation, RCR value increased by 22% and 32% with 1 μM **3a** and 0.5 μM **3b**, respectively (Fig. 1A).

3a and **3b** compounds (Fig. 1B) differ for a nitro group and together with the phenyl rings are suitable for forming π–π and dipole-dipole interactions with biomolecules. Different small molecules can bind F_1 domain (Fig. 1B) and the F_1F_O-ATPase, which is the main candidate component of mPTP, might be the mitochondrial target of Tzs. The inhibitory effects of 1 μM **3a**, 0.5 μM **3b**, and of F_1 domain-specific inhibitors (*i.e.* 75 μM NBD-Cl, 0.8 mM resveratrol, and 0.2 mM piceatannol) on Ca^{2+}-dependent F_1-ATPase activity were documented in partially purified F_1 domain obtained from swine heart mitochondria (Fig. 1C). Conversely, 3 μg/mL oligomycin, a specific inhibitor of F_O domain, was unable to block the ATP hydrolysis in the purified F_1 domain. ATP hydrolysis insensitive to oligomycin on the purified F_1 domain confirmed that the hydrophobic F_O domain was not functionally and structurally linked to the hydrophilic F_1. Moreover, the identification of the β subunit (MW 51.7 kDa) by western blot analyses confirmed the presence of F_1 domain (Fig. 1C), whereas the ATPase (in)sensitivity to specific inhibitors of F_1F_O-ATPase established that the purified fraction containing the F_1 domain was detached from the membrane-embedded F_O domain.

Tzs compounds can bind the F_1 domain. Mutual exclusion analyses were performed with binary mixtures of **3a** or **3b** plus an inhibitor of F_1 domain (iF_1) to identify the binding region of Tzs compounds. Tz plus iF_1 can combine with the enzyme (*E*) to form the ternary *E*-Tz-iF_1 complex or only the binary complex if Tz and iF_1 are mutually exclusive, indicating that one inhibitor prevents the binding of the other inhibitor on F_1F_O-ATPase. Resveratrol (RES) is a phytopolyphenol that interacts with the hydrophobic pocket of F_1 domain formed by the γ subunit and the β_{TP} subunit as depicted in the position of the RES in the crystal structure [45] (Fig. 1D). The reciprocal of F_1F_O-ATPase activity in the presence or in the absence of fixed RES concentrations was plotted as a function of increasing **3a** or **3b** concentrations. In each plot, two straight lines intersecting above the *x* axis in the presence of **3a** or **3b** were obtained (Fig. 1D). This result depicts a simultaneous interaction of **3a** or **3b** and RES with the enzyme, and, therefore, the formation of the ternary complex (*E*-Tz-RES). The intercept of the straight lines represents the values of $\alpha K'_i$, *i.e.* the dissociation constant of the ternary complex. The interaction constant (α) between two different compounds bound to the enzyme obtained from the $\alpha K'_i$ to K'_i ratio indicates whether the binding of one iF_1 affects ($\alpha \neq 1$) or does not affect ($\alpha = 1$) Tzs binding to *E*. The $\alpha < 1$ suggests a synergistic effect between RES and **3a** or **3b** (Fig. 1D). Therefore, one Tz increases the binding constant for the RES.

To verify the possible interaction of Tzs with the catalytic sites of the F_1 domain, binaries mixtures of **3a** or **3b** and NBD-Cl were performed (Fig. 1E). The inhibitory mechanism carries out with NBD-Cl covalent bond to Tyr_{311} of β subunit in empty conformation, without bound nucleotide, can form a NBD-binding pocket within the structure of F_1 domain [46] Fig. 1E. Inhibition kinetic analysis highlighted a different effect of Tzs compounds. The simultaneous interaction of **3a** and NBD-Cl with the F_1F_O-ATPase formed the ternary *E*-**3a**-NBD complex and the α constant obtained from the $\alpha K'_i$ value indicates a mutually cooperative inhibitors binding. Conversely, **3b** and NBD-Cl were mutually exclusive inhibitors in the interaction with the enzyme. The plot depicted parallel straight lines in which the slopes were independent of the presence or absence of **3b** compound (Fig. 1E). Tyr residues could be the molecular target of **3b**. Tetranitromethane (TNM) is a nitrating reagent for Tyr and it has been tested to verify the inhibitory effect of **3b** with and without TNM (Fig. 1F). **3b** and TNM were mutually exclusive. Thus, the F_1F_O-ATPase can combine with either **3b** or TNM, but not with both. Modification of Tyr residues by **3b** has been evaluated based on the formation of nitrotyrosine and/or dityrosine. We evaluated both nitrotyrosine and dityrosine contents in mitochondria incubated with increasing **3b** concentrations. A significant formation of dityrosine above 1.7 nmol **3b**/μg mitochondrial protein was promoted, whereas the level of nitrotyrosines was undetectable (Fig. 1F).

Docking analysis of azide binding site filled with **3a** or **3b** suggested the propensity of **3a** to interact with the azide binding region (Fig. 2). Indeed, azide structure partially resembles the triazole core of compound **3a**. Binary mixtures of **3a** plus azide showed a Dixon-like plot with parallel straight lines according to mutual exclusion (Fig. 1G). Therefore, **3a** displaces the azide from its binding site.

3.2. The 3a and 3b compounds inhibit the mPTP opening

Next, we aimed to address the functional consequences of the specific Tzs binding to the F_1 domain of Ca^{2+}-activated F_1F_O-ATPase, in terms of mPTP inactivation. Ca^{2+} retention capacity (CRC) decreased when the mPTP opened and was revealed by an increase in fluorescence intensity. Likewise, the mitochondrial transmembrane potential (Δϕ) was abruptly dissipated by mPTP opening and was detected by the JC-10 ratio increase. CRC and Δϕ were evaluated upon subsequent 10 μM Ca^{2+} additions at 1 min intervals to succinate-energized freshly-prepared mitochondrial suspensions (Fig. 3 A). In control mitochondria, the rise in the Fura-FF ratio was obtained when the threshold matrix Ca^{2+} concentration load formed mPTP. Similarly, Δϕ collapse in Ca^{2+}-treated mitochondria reflected the membrane depolarization ascribed to mPTP opening. CRC and Δϕ decreased before the third Ca^{2+} pulse in control mitochondria. Conversely, mPTP formation detected by simultaneous measurement of these two different mitochondrial parameters, which were altered when mPTP opened, pointed out that 1 mM **3a** or 0.5 mM **3b** desensitized mPTP formation to Ca^{2+} (Fig. 3 A). Specifically, in isolated mitochondria, **3b** inhibited mPTP more than **3a**.

Then, we wanted to confirm the inhibitory effects of Tzs on mPTP activity observed in isolated mitochondria also in intact AC16 cells, through multiple approaches [42]. Firstly, we monitored Δϕ following addiction to the calcium ionophore ionomycin. Untreated cells showed a gradual decrease in mitochondrial transmembrane potential in response to ionomycin, which reflected the opening of mPTP, whereas both **3a** and **3b** completely prevented Ca^{2+}-dependent mitochondrial depolarization (Fig. 3B,C,D), thus indicating inhibition of mPT. Standard cobalt-calcein assay confirmed that both **3a** and **3b** attenuate mPTP activation in response to ionomycin (Fig. 3E). Moreover, analysis of the mitochondrial network showed that mPTP opening induced drastic morphological changes, as evidenced by increased mitochondrial

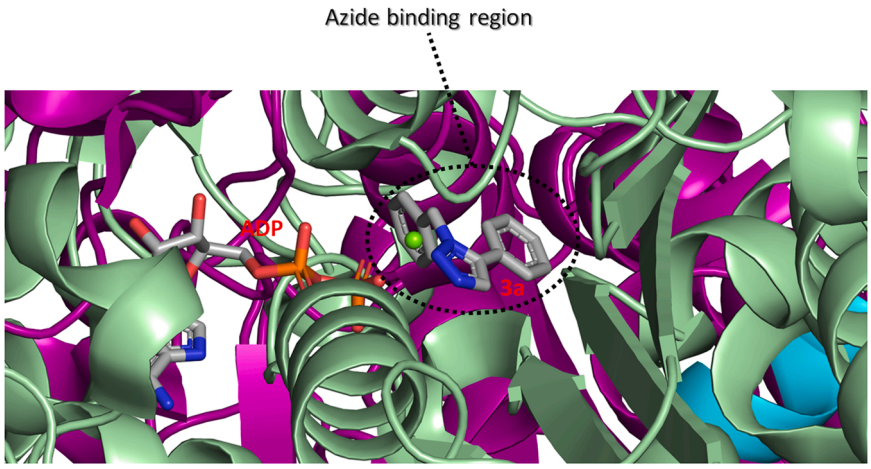

Fig. 2. The docking model of **3a** fitted in the azide binding region of the F_1 domain. The divalent cofactor is represented as a green ball, whereas ATP and **3a** are in stick mode. The α (violet) and β (teal) subunits are drawn by modifying PDB ID code 2CK3.

roundness and reduction of both length and interconnections between mitochondria (Fig. 3 F,G). Pre-treatment with **3a** and **3b** strongly limited the ionomycin-induced morphological rearrangements (Fig. 3F-G), suggesting the protective role of Tzs. Accordingly, **3a** and **3b** confer resistance to Ca^{2+}-induced mPT and cell death (Fig. 3H). However, using a pro-oxidant agent (hydrogen peroxide) to promote mPTP functions, we observed a slight effect of **3b** compound in defending from cell death (Fig. 4 A) or inhibiting mPTP opening (Fig. 4B), and it failed to preserve the normal mitochondrial morphology (Fig. 4 C,D), whereas **3a** fully maintained its protective role (Fig. 4 A,B,C,D). These data indicate that the intracellular redox status might weaken the binding of **3b** Tz with the F_1 domain, thereby loosening its regulatory role on mPTP activity.

In summary, we showed that Tzs inhibit mPT and cell death by limiting the mPTP opening, especially induced by Ca^{2+} ions, and minimizing mitochondrial damage.

3.3. *Tzs protect viability and metabolism of vascular endothelial cells upon hypoxia-reoxygenation*

Porcine aortic endothelial cells (pAEC) viability was evaluated in the presence of increasing doses of **3a** and **3b** after 1 h of incubation. MTT results showed a significant reduction of cell viability (about 35% *vs* CTR) when cells were exposed to **3a** starting from the dose 1 μM. No effect on cell viability was detected in cells exposed to increasing doses of **3b** (Fig. 5A,B). The OXPHOS and glycolysis ATP production in the presence of **3a** or **3b** were evaluated under basal metabolic conditions by measurement of OCR and ECAR values to obtain mitoATP and glycoATP production rate, respectively (Fig. 5C). Tzs did not modify the ATP synthesis of pAECs. Also the ratio between mitoATP Production Rate and glycoATP Production Rate (ATP Rate Index) was always > 1, ensuring a propensity toward mitochondrial oxidative metabolism independently of Tzs treatment (Fig. 5D). The two concentrations used for **3a** and **3b** compounds did not affect the profile and function of cellular respiration of pAECs (Fig. 5E). The key parameters of cell metabolism, which were obtained from OCR values of functional metabolic profile, either in the presence or in the absence of Tzs at the tested concentrations, did not differ from the control (Fig. 5F).

The protective effect of Tzs on pAECs' viability was investigated after the *in vitro* hypoxia/reoxygenation (H/R) injury. H/R injury caused a significant decrease of pAEC viability. MTT results showed that lower doses of both **3a** (0.1 and 0.5 μM) and **3b** (0.1 μM) were not sufficient to recover cell viability after H/R. In contrast, higher doses of both **3a** (1 μM) and **3b** (0.5 and 1 μM) were able to restore significantly cell viability, even though this parameter remained below the control group (Fig. 5G). The impact of H/R on pAECs was characterized by considering the mitochondrial bioenergetic metabolism and highlighting a reduction of OCR value compared with control (in the absence of H/R). Notably, H/R-injured pAECs restored a respiratory profile similar to that of control in the presence of either 1 μM **3a** or 0.5 μM **3b** (Fig. 5H). All key parameters of mitochondrial activities, except the spare respiratory capacity, were decreased upon H/R compared to control. Of interest, we detected an increase of 120% or 93% for basal respiration, of 110% or 95% for proton leak, of 123% or 100% for maximal respiration, and of 130% or 92% for ATP turnover, respectively, in the presence of 1 μM **3a** or 0.5 μM **3b** compared with H/R alone. However, Tzs did not allow to reach the OCR values of the control mitochondrial parameters in H/R injured cells. Conversely, the spare respiratory capacity was only increased by 170% and 150% with **3a** or **3b**, respectively, as compared to baseline metabolism in control or H/R alone (Fig. 5I).

3.4. *Tzs counteract saline load-induced injury in SHRSP cerebral endothelial cells*

We tested the effects of **3a** and **3b** in primary cerebral endothelial cells (ECs) isolated from the stroke-prone spontaneously hypertensive rat (SHRSP), a suitable model for the study of hypertension-related stroke [47–49]. We exposed ECs to high-salt treatment (20 mM NaCl for 72 hrs) either in the presence or in the absence of **3a** or **3b**. We first investigated mitochondrial function by assessing the activity of mitochondrial C-I. High-salt exposure decreased the NAD^+:NADH ratio, as an index of mitochondrial C-I dysfunction, similarly to previous evidence obtained in the SHRSP [39,50]. Both **3a** and **3b** were able to rescue C-I activity in ECs exposed to NaCl (Fig. 6 A).

We also found that **3a** and **3b** improved the cell viability in ECs exposed to high-salt treatment (Fig. 6B). Both **3a** and **3b** also showed protective effects toward the high-salt dependent impairment of angiogenesis. In fact, we found that **3a** and **3b** rescued the endothelial capability to form vessel-like tubes on a matrigel substrate in the presence of high-salt loading (Fig. 6 C,D).

Finally, we tested whether **3a** and **3b** were able to restore vascular function in vessels isolated from SHRSP fed for 4 weeks with a high-salt Japanese style diet (JD). The latter is a dietary regimen able to accelerate stroke occurrence in the SHRSP [39,44,48] by promoting vascular dysfunction [49]. To this aim, vessels isolated from the JD-fed SHRSP were exposed *ex-vivo* with either **3a** or **3b** (Fig. 6E). We observed that JD impaired endothelial-dependent vasorelaxation, in line with our previous evidence [44,49]. Both **3a** and **3b** were able to rescue vascular function in vessels from JD-treated SHRSP (Fig. 6E,F).

Overall, our data suggest that both **3a** and **3b** represent a valid

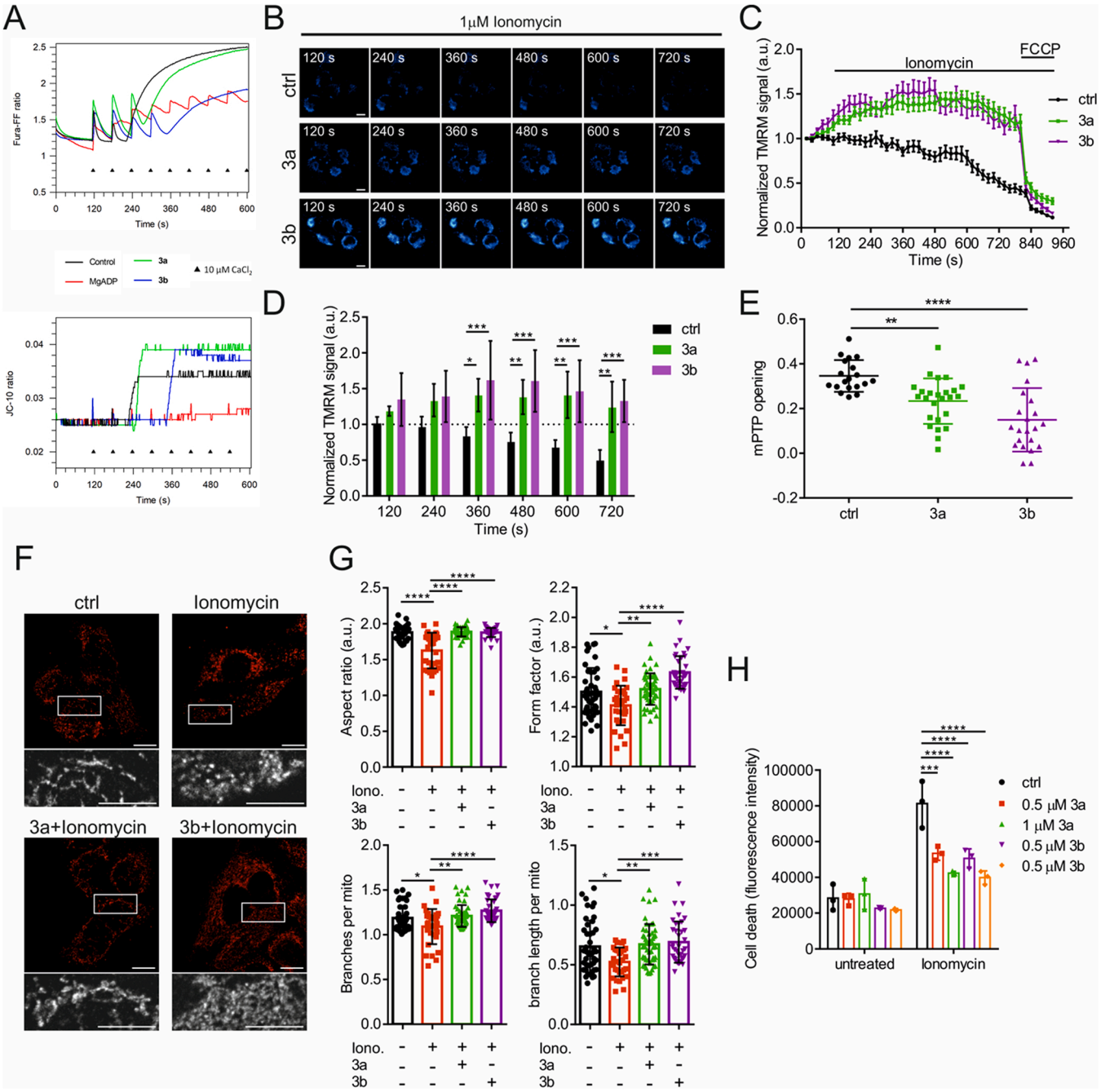

Fig. 3. **3a** and **3b** compounds attenuate mPTP activation. A) Representative plots reporting the ~~E~~evaluation of the mPTP opening and membrane potential in isolated mitochondria. The CRC and Δϕ expressed as the Fura-FF ratio (Fura-FF high Ca^{2+}/Fura-FF low Ca^{2+}) and JC-10 ratio (JC-10 aggregate/JC-10 monomers), respectively, were evaluated in response to subsequent 10 μM $CaCl_2$ pulses (shown by the triangles) in untreated mitochondria (control), and in the presence of 2 mM MgADP, 1.0 mM compound 3a, 0.5 mM compound **3b**. N = 3 independent experiments. B) Representative images of AC16 cells loaded with the mitochondrial membrane potential sensitive fluorescent probe TMRM and then treated with 1 μM ionomycin; where indicated, cells were pre-treated for 30 min with 1 μM **3a** or **3b**, before addiction of ionomycin. Scale bar: 10 μm C) Kinetics of time-dependent changes of TMRM signal, related to Fig. 3B. N = 4 independent experiments; mean ±SEM. D) Statistical analysis of the experiments showed in Fig. 3B-C, reporting the normalized TMRM values at different time points upon addiction of ionomycin. N = 4 independent experiments; mean±SD. E) Calcein-cobalt quenching assay of AC16 cells, for which mPTP activity is reported as the drop in calcein fluorescence before and after 10 min of 1 μM ionomycin. N = 3 independent experiments (>20 fields per condition); mean±SD. F) Representative morphological images of the AC16 mitochondria treated or not with 1 μM ionomycin. Where indicated, cells were pre-treated for 30 min with 1 μM **3a** or **3b**. The white boxes indicate a specific region of the mitochondrial network magnified in the insets shown at the bottom. Scale bar: 10 μm. G) Analysis of mitochondrial morphology, evaluated through comparison of mitochondrial morphometry parameters (aspect ratio and form factor) and mitochondrial network connectivity (branches per mitochondria and branches lenght). N = 3 independent experiments (>35 cells per condition); mean±SD. H) Cell death quantification of AC16 cells after 1 h of treatment with 1 μM ionomycin, pre-treated or not with **3a** or **3b** at the indicated concentrations. N = 3 independent experiments; mean±SD.

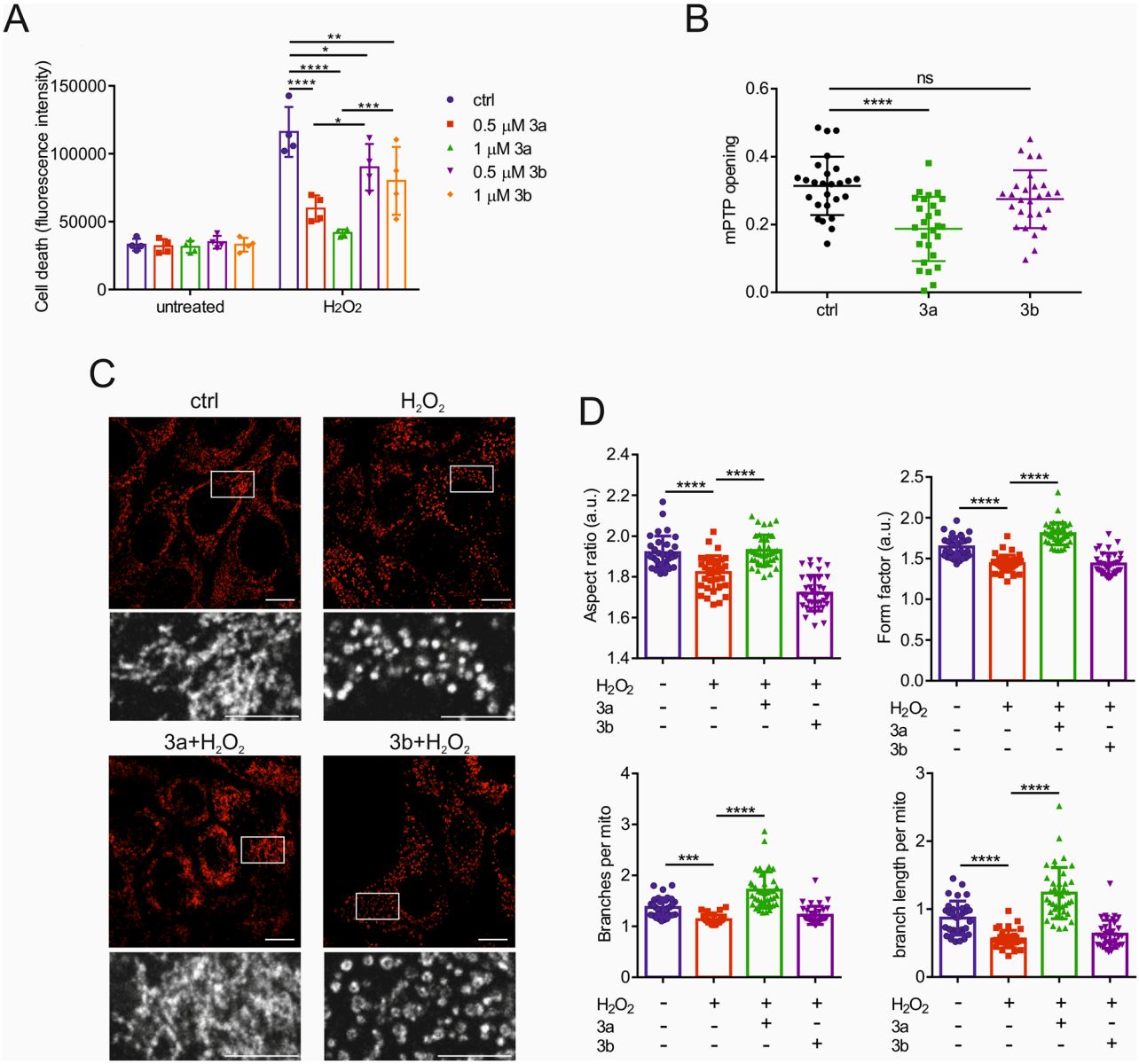

Fig. 4. 3b triazole showed lower protective effects in response to hydrogen peroxide. A) Cell death quantification of AC16 cells after 1 h of treatment with 250 μM H_2O_2, pre-treated or not with **3a** or **3b** at the indicated concentrations. N = 3 independent experiments; mean±SD. B) Calcein-cobalt quenching assay of AC16 cells, for which mPTP activity is reported as the drop in calcein fluorescence before and after 10 min of 250 μM H_2O_2. N = 3 independent experiments (>25 fields per condition); mean±SD. C) Representative morphological images of the AC16 mitochondria treated or not with 250 μM H_2O_2. Where indicated, cells were pre-treated for 30 min with 1 μM **3a** or **3b**. The white boxes indicate a specific region of the mitochondrial network magnified in the insets shown at the bottom. Scale bar: 10 μm. D) Analysis of mitochondrial morphology, evaluated through comparison of mitochondrial morphometry parameters (aspect ratio and form factor) and mitochondrial network connectivity (branches per mito and branches length). AC16 cells were treated or not with 250 μM H_2O_2; where indicated, cells were pre-treated for 30 min with 1 μM **3a** or **3b**. N = 3 independent experiments (>35 cells per condition); mean±SD.

intervention to improve endothelial function in a model of stroke associated with hypertension. The observed improvement of NAD^+:NADH ratio following either **3a** or **3b** administration also confirms that mitochondrial impairment represents a key molecular determinant of endothelial dysfunction in response to the high-salt treatment.

4. Discussion

Our results demonstrate that 1,5-disubstituted-1,2,3-triazoles inhibit mPTP opening by acting on F_1F_O-ATPase and protect vascular cells from damage.

Mitochondrial dysfunction is a typical feature of CVDs, although the available information does not allow a conclusive elucidation of causal relationships. The essential functions of mitochondria in eukaryotic cells support ATP synthesis, calcium homeostasis, oxidative stress response, and regulated cell death [51]. In the pathophysiology of CVDs, damaged mitochondria could cause serious consequences and even lead to cell death [52]. Mitochondrial homeostasis or dysfunctions are dependent on short/long-lasting mPTP opening events [53]. In the attempt to identify possible clinical applications that block mPTP formation, we need also to consider the potential adverse effects of prolonged mPTP inhibition in failing hearts [54]. Indeed, mPTP opening rises as the initial compensation or the eventual deregulation events that bear to the structural/functional alterations in CVDs [55]. Recent results on mPTP assert the existence of two channels. The long-standing hypothesis that the mPTP could form from the adenine nucleotide translocator (ANT)

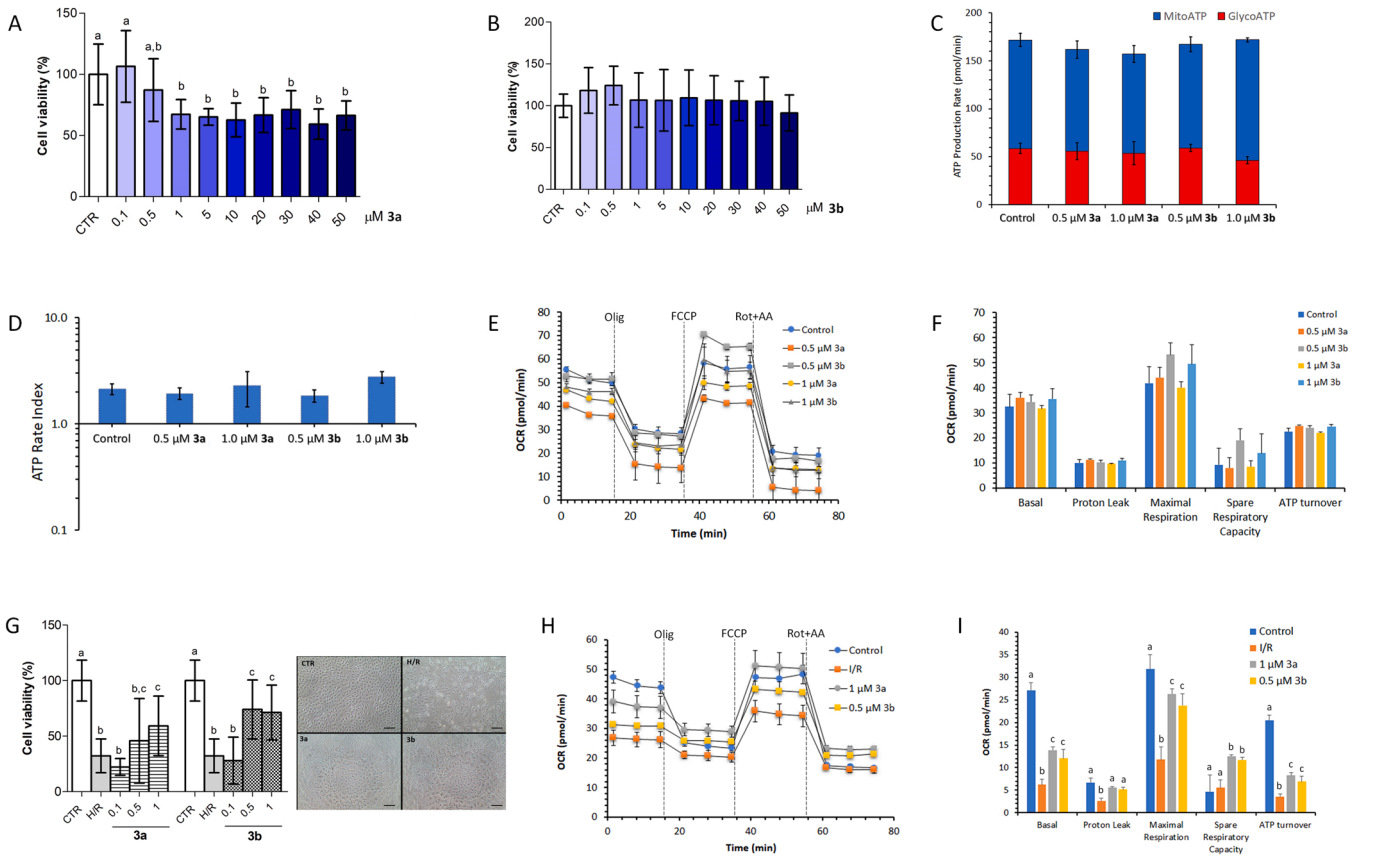

Fig. 5. Evaluation of cell viability and cell metabolism in the presence of Tz compounds and protective effect from hypoxia/reoxygenation (H/R) injury. Cells were treated with different doses of **3a** (A) or **3b** (B). C) The real-time ATP production rate in pAECs. Evaluation of ATP production rate by mitochondrial OXPHOS (blue) or by glycolysis (red) in Tzs-treated cells. D) The ATP rate index is shown on the *y*-axis (logarithmic scale) in pEACs treated without (control) and with the Tzs. E) The mitochondrial respiration profile was obtained from the OCR without and with Tzs under basal respiration conditions and after the addition of 1.5 μM oligomycin (olig), 1.0 μM FCCP, and a mixture of 0.5 μM rotenone plus antimycin A (Rot+AA). Inhibitor injections are shown as dotted lines. F) Mitochondrial parameters (basal respiration, ATP production, proton leak, maximal respiration, spare respiratory capacity, non-mitochondrial oxygen consumption, ATP turnover) in the absence or in the presence of **3a** or **3b**. G) Effect of the **3a** and **3b** on H/R injured pAEC's viability and morphology. Scale bar (–) 100 μm. Different letters above the bars indicate significant differences ($P \leq 0.05$, one-way ANOVA, *post hoc* Tuckey comparison test) between H/R treatment with and without Tzs and the control (CTR) group. H) H/R effect on mitochondrial respiration profile and (I) on mitochondrial parameters in the absence or in the presence of **3a** or **3b**. Data expressed as column charts (A, B,C,D,F,G,I) or points (E,H) represent the mean±SD (vertical bars) from four experiments carried out on different cell preparations. Different letters indicate significant differences ($P \leq 0.05$) among treatments within the same parameter from at least five experiments carried out on different cell preparations.

has been re-evaluated. Indeed, the ANT-dependent mPTP activity can be activated independently of cyclophilin D (CyPD), a key modulator of mPTP, in response to higher mitochondrial matrix Ca^{2+} levels [56]. This channel has a significantly lower conductance compared with CyPD-sensitive pore [57]. Conversely, a large conductance channel activity might originate from Ca^{2+}-dependent conformational change of the F_1F_O-ATPase [58,59]. Cryo-EM of Ca^{2+}-activated F_1F_O-ATPase has led to a model of mPTP formation. After several disputes, the *c*-ring of the enzyme has been suggested to house the leak channel of the mPT [57,58,60–62]. In mitochondrial biology, a new scenario for the F_1F_O-ATPase has started and the multiple enzyme functions dwell in the membrane-embedded F_O domain [63]. The model asserts mPTP opening with the displacement of F_1 from F_O in Ca^{2+}-activated F_1F_O-ATPase oligomeric state. Ca^{2+} bound to the catalytic sites of the enzyme induces conformational changes in the F_1 domain that are transmitted through the peripheral stalk to the F_O domain. The subsequent structural conformations might pull out/displace the lipid plugs from the hole of the *c*-ring. The *c*-ring lumen expands during these events and mPTP opens. Electrophysiological studies have defined the gating mechanism of the *c*-ring in mPTP formation with the proposal of the "bent-pull-twist" model confirming the role of the enzyme in the mPTP formation [11]. The pharmacophores approach, aiming at selecting the molecular features of compounds recognized by specific biological macromolecules, reveals the inhibition of Ca^{2+}-activated F_1F_O-ATPase to block mPTP formation without affecting the activity of ATP synthesis sustained by Mg^{2+}-activated enzyme [64].

The mPTP opening implies that the IMM integrity is lost and mitochondria do not retain the ion homeostasis. The ability of **3a** and **3b** compounds to counteract the mPTP formation in isolated heart mitochondria is evaluated using the CRC, which measures the capability of intact mitochondria to accumulate Ca^{2+}, and the detection of $\Delta\phi$ – known as the electrical component of the mitochondrial protonmotive force – (Fig. 3 A). In general, Tz compounds are counted as potential mPTP inhibitors [14,15,20,65] and the F_1F_O-ATPase has been identified as the molecular target. As a component of the OXPHOS system, the ATP synthesis could be impaired in the presence of Tzs. However, it was ascertained that **3a** or **3b** did not significantly affect the mitochondrial respiration in glutamate/malate- or succinate-energized mitochondria [14] and Tzs cannot reduce the electron flow in the OXPHOS system. The Tzs interaction with Mg^{2+}-activated F_1F_O-ATPase takes place without affecting ATP synthesis. Moreover, the coupling between glutamate/malate oxidation and ADP phosphorylation, evaluated as the state 3/state 4 ratio, was improved by Tzs (Fig. 1A). The results corroborate the hypothesis that specific inhibition of Ca^{2+}-activated F_1F_O-ATPase and the refractivity to the Tz compounds of the F_1F_O-ATPase activated with the natural cofactor Mg^{2+}, highlight the link

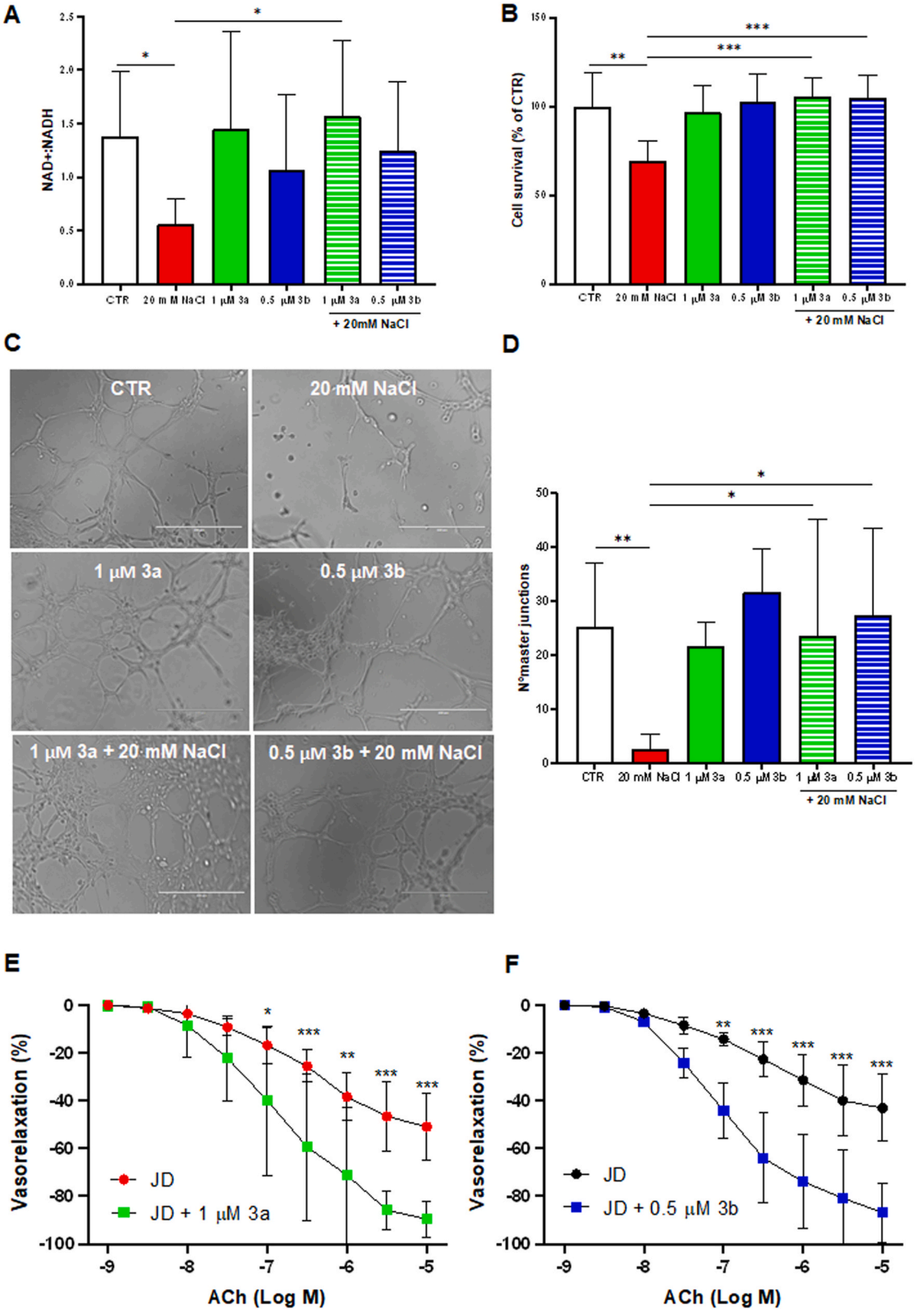

Fig. 6. **3a** and **3b** exert beneficial effects on ECs and vascular function in the stroke-prone spontaneously hypertensive rat (SHRSP). Cerebral ECs were isolated from the brain of the SHRSP and treated for 72 h with 20 mM NaCl, either in the absence or in the presence of **3a** (1 μM) or **3b** (0.5 μM). The effects of **3a** and **3b** were evaluated on NAD^+:NADH ratio ($N = 5–9$) (A), cell viability ($N = 6$) (B) and angiogenesis ($N = 3–6$) (C-D). Representative images of matrigel assay (C) and quantification of master junctions (D). * $P < 0.05$, * * $P < 0.01$, * ** $P < 0.001$ obtained by One-way ANOVA followed by Bonferroni's *post hoc* test. E-F. Mesenteric arteries isolated from SHRSP receiving Japanese style diet (JD) for 4 weeks were treated *ex vivo* with **3a** (1 μM) (E) or **3b** (0.5 μM) (F) for 1 h (N = 4). * $P < 0.05$ * * $P < 0.01$ and * ** $P < 0.001$ were obtained by using 2-way ANOVA followed by Bonferroni's multiple comparison test. Data in the figure are reported as mean±SD.

between Ca^{2+}-activated F_1F_O-ATPase and mPTP formation [13,66]. Understanding the molecular mechanism of action of Tzs on Ca^{2+}-activated F_1F_O-ATPase/mPTP axes is needed to succeed in identifying the possible binding region of compounds. Significant enzyme inhibition has been detected on Ca^{2+}-activated F_1F_O-ATPase by **3a** or **3b**, whereas the same compounds did not affect Mg^{2+}-activated enzyme [14]. The different effects on the two differently activated F_1F_O-ATPases could be attributed to enzyme conformations promoted by Ca^{2+} or Mg^{2+} cofactor bound to the catalytic and/or noncatalytic sites of the F_1 domain. Thus, the F_1 might be the binding region of Tzs. Indeed, Ca^{2+}-dependent ATP hydrolysis of the purified F_1 domain was sensitive to Tzs. In order to establish the possible binding sites(s) of **3a** and **3b** compounds, multiple inhibition analyses with binary mixtures of Tzs and inhibitors of the F_1 domain, with known binding sites, were performed. As a result, **3a** or **3b** and RES did not mutually exclude and can form the ternary *E*-Tz-RES complex (Fig. 1D). Therefore, Tzs bind to a different site from the RES in the F_1 domain. NBD-Cl and TNM, two different Tyr-reagents, were mutually exclusive inhibitors with **3b**. The inhibition caused by either NBD-Cl or TNM was prevented by **3b** since Ca^{2+}-activated F_1F_O-ATPase can combine with Tyr-reagent or **3b** but not with both (Fig. 1E,F). The main difference between **3a** and **3b** is the presence of nitrite group of the latter. Modification of tyrosine residues by nitrite can lead to the formation of nitrotyrosine and/or dityrosine [67] and **3b** only promotes a significant formation of dityrosine (Fig. 1F). Therefore, the putative Tyr-311 covalently bond with NBD-Cl [46] and Tyr-349 or Tyr-372 nitrated by TNM could be modified by **3b**. The ditryrosine **3b**-dependent post-translational modification (PTM) might arise between Tyr residues that show electron tunnelling redox distance less than 14 Å needed to support electron transfer [68]. Nitrite would possess both anti- and pro-oxidant activities and nitrite group of **3b** could transfer one electron to the enzyme to form two adjacent tyrosyl radicals bound together to form dityrosine [25]. Candidate Tyr residues to support PTM in the NBD-Cl binding region with a distance lower than 14 Å might be Tyr-335 or Tyr-281 of α and β subunits, respectively (Fig. 7A). TNM can interact with Tyr-349 or Tyr-372 of the β subunit, but only the former has a Tyr residue (Tyr-462) that supports the electron tunnelling (Fig. 7B).

Docking analysis suggests that the active site of azide fits the structure of **3a** (Fig. 2). Likewise, multiple inhibition analyses with binary mixtures of azide, known to block ATP hydrolysis when Pi leaves the catalytic site [69], and **3a** indicated that the compounds are mutually excluded (Fig. 1G). Therefore, **3a** can overlap the azide binding region in the catalytic sites of the F_1 domain.

Using different experimental approaches, we showed that Tzs are able to inhibit mPTP activation, limiting mitochondrial membrane potential dissipation and avoiding mitochondrial swelling, thus preserving normal mitochondrial morphology. All these events concur to protect cardiomyocytes from extensive cell death induced by calcium agents (Fig. 3). Intriguingly, **3b** compound is less effective when mitochondria are exposed to oxidative stress (Fig. 4). This event might be explained, at least in part, by the redox activity of the nitrite group of **3b**. The compound interacting with the hydrogen peroxide might produce a scavenger effect that allows the dityrosine formation. Indeed, nitrite group of **3b** compound upon oxidative stress might accept one electron from ROS to form the radical·NO_2, which can nitrate tyrosine residues and form other radical species [70] (*e.g.*, tyrosyl radical). During ATP hydrolysis two adjacent tyrosyl radicals bind together and can form dityrosine [67]. The dityrosine formation seems to be especially deleterious for ATPase activity sustained by Ca^{2+}-activated F_1F_O-ATPase [25] that, consequently, blocks mPTP formation [13].

pAECs represent a good translational model to study the endothelial dysfunction related to impaired mitochondrial physiology during CVDs. Endothelial cells contain fewer mitochondria than cardiomyocytes, and several of the pathological alterations during H/R injury involve mitochondria. The infarct zone is determined by vascular obstruction and endothelial cell injury may occur earlier than in cardiomyocytes [71]. Anaerobic metabolism of the endothelial cells allows for tolerating periods of ischemia. Otherwise, this feature makes the endothelial cells particularly vulnerable during reperfusion when mitochondrial homeostasis is disrupted, even if the reintroduction of oxygen could restart OXPHOS. Nevertheless, the mitochondrial electron transport chain, increasing the generation of ROS and mitochondrial Ca^{2+} overload, compromises cellular energetics with the mPTP opening [72]. The capability of Tzs to prevent mPTP formation has been exploited to verify the cardiovascular protective function of these compounds. However, before testing Tzs effects on *in vitro* H/R damage, the cytotoxic analysis of cell viability and cell metabolism was evaluated in order to verify the absence of the inhibitory effect of Tzs on cell metabolism at the concentration used to perform the H/R experiments. As a result, cell viability under Tzs treatment was structure- and dose-dependent with an unfavourable response at increasing **3a** concentrations. To examine cell metabolism toxicity, we analyzed the OCRs using Seahorse XFp extracellular flux analyzer and evaluated the ATP production and the mitochondrial bioenergetic parameters. Importantly, **3a** or **3b** did not exhibit any adverse effects on pAECs metabolism (Fig. 5A-F). Together, these results demonstrated that Tzs were not toxic to mitochondria activity or cell energy metabolism. The *in vitro* evaluation of the H/R effect on cell viability highlighted the injury occurring during reperfusion. On the other hand, cell viability was preserved in the presence of **3a** or **3b** (Fig. 5G). The detrimental effect of H/R on cell viability might be correlated with the impaired bioenergetics of cell metabolism since the decrease in mitochondrial parameters was joined to OXPHOS dysfunction. Indeed, mitochondria respiration and ATP synthesis decreased as a possible consequence of mPTP formation. However, **3a** or **3b** preserved the basal and maximal respiration, the proton leak and the ATP turnover or improved spare respiratory capacity (Fig. 5H,I) suggesting that the mitochondria are the molecular targets of Tzs compounds in pAECs.

The SHRSP represents a well characterized suitable model for studies

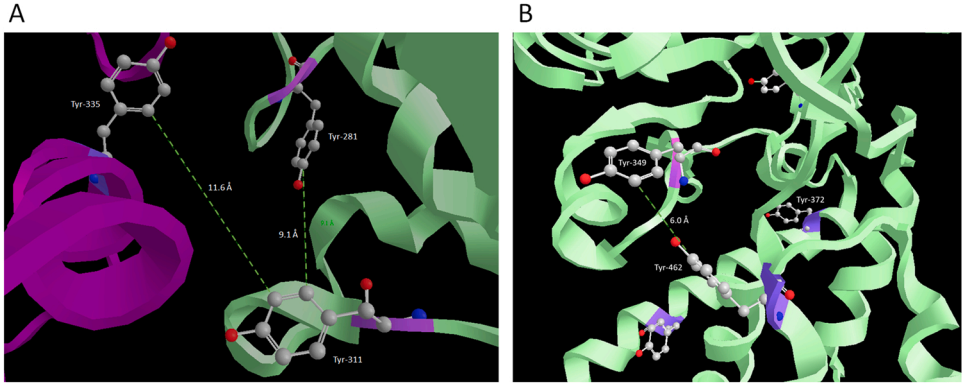

Fig. 7. The spatial arrangement of Tyr residue of F_1 domain candidate to support the dithyrosine adduct. A) The panel illustrate the βTyr-311 and the putative βTyr-281 or αTyr-311 able to form dithyrosines. B) The panel highlight βTyr-462 that might interact with βTyr-349. The calculated distances between the aromatic ring of Tyr residues are reported as green lines. The α (violet) and β (teal) subunits are drawn by modifying PDB ID code 6TT7. Tyr residues are drawn in the ball and stick model.

on human hypertensive disease and related vascular damage [73]. In particular, this model accelerates stroke occurrence under a high-salt/low potassium diet, and develops, at the molecular level, a severe mitochondrial C-I dysfunction due to Ndufc2 subunit inhibition [50]. To mimic the *in vivo* condition, we exposed primary cerebral ECs obtained from SHRSP pups to saline load and detected an impaired C-I mitochondrial function, reduced cell viability and endothelial cell tubes formation on Matrigel assay. Exposure to **3a** and **3b** resulted in significant protection from the high-salt induced cell injury (Fig. 6); indeed, **3a** and **3b** promoted the OXPHOS in isolated mitochondria during glutamate/malate oxidation (Fgure 1 A). In accordance, Tzs restored in a significant manner the impaired endothelial-dependent vascular relaxation in high-salt fed SHRSP rats. The whole set of data performed in this experimental context, while further underlying the pathogenetic role of C-I dysfunction in stroke-related vascular abnormalities and mPTP formation in regulated cell death [50,74], underscores the key role of Tzs as an intriguing promising tool for prevention and treatment. Based on these relevant results, the potential beneficial effects of **3a** and **3b** on stroke survival need to be tested *in-vivo* in the SHRSP.

On balance, we have identified the catalytic activity of the F_1F_O-ATPase stimulated by Ca^{2+} as the molecular event counteracted by Tzs to block mPTP formation. The regulation of this biological phenomenon by small molecules can avoid the cardiovascular dysfunction raised by dysfunctional and damaged mitochondria and encourage drug discovery based on the possible bioarchitecture of mPTP [64].

CRediT authorship contribution statement

S.M., S.R. and S.N. Conceptualization; C.B., M.A.T., F.B., F.D.N., and R.S. Methodology; C.A., S.M., M.F., D.L.M., V.A., R.S. and S.N. Investigation; C.A., S.M., C.B., S.R. and S.N. Validation; F.B., M.C., F.T. and P.C. Resources; S.M., R.S. and S.N. Writing – original draft; F.T., L.M., M.F., A.D.N., F.D.N., S.S and M.V. Writing – review & editing; M.F., S.M. and S.N. Visualization; M.V., S.R. and S.N. Supervision; S.R. and S.N. Funding acquisition.

Declaration of Competing Interest

The authors declare the following financial interests/personal relationships which may be considered as potential competing interests: Salvatore Nesci reports financial support was provided by University of Bologna. Speranza Rubattu reports financial support was provided by Italian Ministry of Health.

Data Availability

The data that has been used is confidential.

Acknowledgments

Danilo Matteuzzi and Roberto Giusti (Department of Veterinary Medical Sciences, University of Bologna) are gratefully acknowledged for kindly conferring swine hearts from a local slaughterhouse to Biochemistry laboratories. This work was financed by the University of Bologna, RFO 2020 grant to SN, by a grant from the Italian Ministry of Health to SR, by Progetto PRIN 2017 (from the Italian Ministry of Instruction, University and Research, n. 2017PZY5K7) to SR.

Declaration of interests

The authors declare no competing interests.

References

[1] F.J. Bock, S.W.G. Tait, Mitochondria as multifaceted regulators of cell death, Nat. Rev. Mol. Cell Biol. (2019), https://doi.org/10.1038/s41580-019-0173-8.

[2] S. Nesci, F. Trombetti, A. Pagliarani, V. Ventrella, C. Algieri, G. Tioli, G. Lenaz, Molecular and supramolecular structure of the mitochondrial oxidative phosphorylation system: implications for pathology, Life 11 (2021) 242, https://doi.org/10.3390/life11030242.

[3] M. Bonora, C. Giorgi, P. Pinton, Molecular mechanisms and consequences of mitochondrial permeability transition, Nat. Rev. Mol. Cell Biol. 23 (2022) 266–285, https://doi.org/10.1038/s41580-021-00433-y.

[4] W. Kühlbrandt, Structure and mechanisms of F-Type ATP synthases, Annu. Rev. Biochem. 88 (2019) 515–549, https://doi.org/10.1146/annurev-biochem-013118-110903.

[5] P. Mitchell, Coupling of phosphorylation to electron and hydrogen transfer by a chemi-osmotic type of mechanism, Nature 191 (1961) 144–148.

[6] A. Hahn, K. Parey, M. Bublitz, D.J. Mills, V. Zickermann, J. Vonck, W. Kühlbrandt, T. Meier, Structure of a complete ATP synthase dimer reveals the molecular basis of inner mitochondrial membrane morphology, Mol. Cell. 63 (2016) 445–456, https://doi.org/10.1016/j.molcel.2016.05.037.

[7] B.J. Murphy, N. Klusch, J. Langer, D.J. Mills, Ö. Yildiz, W. Kühlbrandt, Rotary substates of mitochondrial ATP synthase reveal the basis of flexible F1-Fo coupling, Science 364 (2019), https://doi.org/10.1126/science.aaw9128.

[8] W. Junge, H. Sielaff, S. Engelbrecht, Torque generation and elastic power transmission in the rotary F(O)F(1)-ATPase, Nature 459 (2009) 364–370, https://doi.org/10.1038/nature08145.

[9] P. Dimroth, C. von Ballmoos, T. Meier, Catalytic and mechanical cycles in F-ATP synthases. Fourth in the Cycles Review Series, EMBO Rep. 7 (2006) 276–282, https://doi.org/10.1038/sj.embor.7400646.

[10] S. Nesci, Mitochondrial permeability transition, F_1F_O-ATPase and calcium: an enigmatic triangle, EMBO Rep. 18 (2017) 1265–1267, https://doi.org/10.15252/embr.201744570.

[11] N. Mnatsakanyan, H.-A. Park, J. Wu, X. He, M.C. Llaguno, M. Latta, P. Miranda, B. Murtishi, M. Graham, J. Weber, R.J. Levy, E.V. Pavlov, E.A. Jonas, Mitochondrial ATP synthase c-subunit leak channel triggers cell death upon loss of its F1 subcomplex, Cell Death Differ. (2022), https://doi.org/10.1038/s41418-022-00972-7.

[12] S. Nesci, What happens when the mitochondrial H+-translocating F1FO-ATP (hydrol)ase becomes a molecular target of calcium? The pore opens, Biochimie 198 (2022) 92–95, https://doi.org/10.1016/j.biochi.2022.03.012.

[13] C. Algieri, F. Trombetti, A. Pagliarani, V. Ventrella, C. Bernardini, M. Fabbri, M. Forni, S. Nesci, Mitochondrial Ca2+ -activated F1 FO -ATPase hydrolyzes ATP and promotes the permeability transition pore, Ann. N. Y. Acad. Sci. 1457 (2019) 142–157, https://doi.org/10.1111/nyas.14218.

[14] V. Algieri, C. Algieri, L. Maiuolo, A. De Nino, A. Pagliarani, M.A. Tallarida, F. Trombetti, S. Nesci, 1,5-Disubstituted-1,2,3-triazoles as inhibitors of the mitochondrial Ca2+ -activated F1 FO -ATP(hydrol)ase and the permeability transition pore, Ann. N. Y Acad. Sci. 1485 (2021) 43–55, https://doi.org/10.1111/nyas.14474.

[15] S. Antonucci, M. Di Sante, J. Sileikyte, J. Deveraux, T. Bauer, M.J. Bround, R. Menabò, M. Paillard, P. Alanova, M. Carraro, M. Ovize, J.D. Molkentin, M. Cohen, M.A. Forte, P. Bernardi, F. Di Lisa, E. Murphy, A novel class of cardioprotective small-molecule PTP inhibitors, Pharmacol. Res. 151 (2019), 104548, https://doi.org/10.1016/j.phrs.2019.104548.

[16] A. De Nino, P. Merino, V. Algieri, M. Nardi, M.L. Di Gioia, B. Russo, M.A. Tallarida, L. Maiuolo, Synthesis of 1,5-functionalized 1,2,3-triazoles using ionic liquid/iron (III) chloride as an efficient and reusable homogeneous catalyst, Catalysts 8 (2018), https://doi.org/10.3390/catal8090364.

[17] L. Maiuolo, B. Russo, V. Algieri, M. Nardi, M.L. Di Gioia, M.A. Tallarida, A. De Nino, Regioselective synthesis of 1,5-disubstituted 1,2,3-triazoles by 1,3-dipolar cycloaddition: Role of Er(OTf)3, ionic liquid and water, Tetrahedron Lett. 60 (2019) 672–674, https://doi.org/10.1016/j.tetlet.2019.01.053.

[18] R. Kharb, P.C. Sharma, M.S. Yar, Pharmacological significance of triazole scaffold, J. Enzym. Inhib. Med Chem. 26 (2011) 1–21, https://doi.org/10.3109/14756360903524304.

[19] N. Singhal, P.K. Sharma, R. Dudhe, N. Kumar, Recent advancement of triazole derivatives and their biological significance, J. Chem. Pharm. Res. 3 (2011) 126–133.

[20] J. Šileikytė, J. Devereaux, J. de Jong, M. Schiavone, K. Jones, A. Nilsen, P. Bernardi, M. Forte, M.S. Cohen, Second-generation inhibitors of the mitochondrial permeability transition pore with improved plasma stability, ChemMedChem 14 (2019) 1771–1782, https://doi.org/10.1002/cmdc.201900376.

[21] P. Bernardi, A. Rasola, M. Forte, G. Lippe, The mitochondrial permeability transition pore: channel formation by F-ATP synthase, integration in signal transduction, and role in pathophysiology, Physiol. Rev. 95 (2015) 1111–1155, https://doi.org/10.1152/physrev.00001.2015.

[22] S. Nesci, GPR35, ally of the anti-ischemic ATPIF1-ATP synthase interaction, Trends Pharmacol. Sci. 43 (2022) 891–893, https://doi.org/10.1016/j.tips.2022.09.003.

[23] G.A. Wyant, W. Yu, Ii.P. Doulamis, R.S. Nomoto, M.Y. Saeed, T. Duignan, J. D. McCully, W.G. Kaelin, Mitochondrial remodeling and ischemic protection by G protein-coupled receptor 35 agonists, Science 377 (2022) 621–629, https://doi.org/10.1126/science.abm1638.

[24] G. Morciano, D. Preti, G. Pedriali, G. Aquila, S. Missiroli, A. Fantinati, N. Caroccia, S. Pacifico, M. Bonora, A. Talarico, C. Morganti, P. Rizzo, R. Ferrari, M. R. Wieckowski, G. Campo, C. Giorgi, C. Trapella, P. Pinton, Discovery of novel 1,3,8-triazaspiro[4.5]decane derivatives that target the c subunit of F1/FO-adenosine triphosphate (ATP) synthase for the treatment of reperfusion damage in myocardial infarction, J. Med. Chem. 61 (2018) 7131–7143, https://doi.org/10.1021/acs.jmedchem.8b00278.

[25] S. Nesci, V. Ventrella, F. Trombetti, M. Pirini, A. Pagliarani, Preferential nitrite inhibition of the mitochondrial F1FO-ATPase activities when activated by Ca(2+) in replacement of the natural cofactor Mg(2+), Biochim. Biophys. Acta 2016 (1860) 345–353, https://doi.org/10.1016/j.bbagen.2015.11.004.
[26] F. Penin, C. Godinot, D.C. Gautheron, Optimization of the purification of mitochondrial F1-adenosine triphosphatase, Biochim. Biophys. Acta 548 (1979) 63–71.
[27] M.M. Bradford, A rapid and sensitive method for the quantitation of microgram quantities of protein utilizing the principle of protein-dye binding, Anal. Biochem. 72 (1976) 248–254.
[28] S. Nesci, V. Ventrella, F. Trombetti, M. Pirini, A. Pagliarani, Tri-n-butyltin binding to a low-affinity site decreases the F1FO-ATPase sensitivity to oligomycin in mussel mitochondria, Appl. Organomet. Chem. 26 (2012) 593–599, https://doi.org/10.1002/aoc.2904.
[29] T. Yonetani, [26] The Yonetani-Theorell graphical method for examining overlapping subsites of enzyme active centers, in: D.L. Purich (Ed.), Methods in Enzymology, Academic Press, 1982, pp. 500–509, https://doi.org/10.1016/S0076-6879(82)87028-6.
[30] S. Nesci, V. Ventrella, F. Trombetti, M. Pirini, A. Pagliarani, Thiol oxidation is crucial in the desensitization of the mitochondrial F1FO-ATPase to oligomycin and other macrolide antibiotics, Biochim. Biophys. Acta 2014 (1840) 1882–1891, https://doi.org/10.1016/j.bbagen.2014.01.008.
[31] O. Trott, A.J. Olson, AutoDock Vina: improving the speed and accuracy of docking with a new scoring function, efficient optimization, and multithreading, J. Comb. Chem. 31 (2010) 455–461, https://doi.org/10.1002/jcc.
[32] Y. Zhao, D.G. Truhlar, The M06 suite of density functionals for main group thermochemistry, thermochemical kinetics, noncovalent interactions, excited states, and transition elements: Two new functionals and systematic testing of four M06-class functionals and 12 other function, Theor. Chem. Acc. 120 (2008) 215–241, https://doi.org/10.1007/s00214-007-0310-x.
[33] G. Scalmani, M.J. Frisch, Continuous surface charge polarizable continuum models of solvation. I. General formalism, J. Chem. Phys. 132 (2010), https://doi.org/10.1063/1.3359469.
[34] G.M. Morris, R. Huey, W. Lindstrom, M.F. Sanner, R.K. Belew, D.S. Goodsell, A. J. Olson, AutoDock4 and AutoDockTools4: Automated docking with selective receptor flexibility, J. Comput. Chem. 30 (2009) 2785–2791, https://doi.org/10.1002/jcc.
[35] C.B., W. Gr, Respiratory enzymes in oxidative phosphorylation. III. The steady state, The Journal of Biological Chemistry. 217 (1955). ⟨https://pubmed.ncbi.nlm.nih.gov/13271404/⟩ (accessed June 13, 2022).
[36] M.A. Neginskaya, S.E. Morris, E.V. Pavlov, Both ANT and ATPase are essential for mitochondrial permeability transition but not depolarization, IScience (2022), 105447, https://doi.org/10.1016/j.isci.2022.105447.
[37] H. Ischiropoulos, A.B. Al-Mehdi, Peroxynitrite-mediated oxidative protein modifications, FEBS Lett. 364 (1995) 279–282, https://doi.org/10.1016/0014-5793(95)00307-U.
[38] C. Bernardini, A. Zannoni, M.E. Turba, P. Fantinati, C. Tamanini, M.L. Bacci, M. Forni, Heat shock protein 70, heat shock protein 32, and vascular endothelial growth factor production and their effects on lipopolysaccharide-induced apoptosis in porcine aortic endothelial cells, Cell Stress Chaperon-.-. 10 (2005) 340–348, https://doi.org/10.1379/csc-98r1.1.
[39] M. Forte, F. Bianchi, M. Cotugno, S. Marchitti, E. De Falco, S. Raffa, R. Stanzione, F. Di Nonno, I. Chimenti, S. Palmerio, F. Pagano, V. Petrozza, A. Micaloni, M. Madonna, M. Relucenti, M.R. Torrisi, G. Frati, M. Volpe, S. Rubattu, S. Sciarretta, Pharmacological restoration of autophagy reduces hypertension-related stroke occurrence, Autophagy 16 (2020) 1468–1481, https://doi.org/10.1080/15548627.2019.1687215.
[40] A. Chaudhry, R. Shi, D.S. Luciani, A pipeline for multidimensional confocal analysis of mitochondrial morphology, function, and dynamics in pancreatic β-cells, Am. J. Physiol. Endocrinol. Metab. 318 (2020) E87–E101, https://doi.org/10.1152/ajpendo.00457.2019.
[41] I.M.G.M. Hemel, B.P.H. Engelen, N. Luber, M. Gerards, A hitchhiker's guide to mitochondrial quantification, Mitochondrion 59 (2021) 216–224, https://doi.org/10.1016/j.mito.2021.06.005.
[42] M. Bonora, C. Morganti, G. Morciano, C. Giorgi, M.R. Wieckowski, P. Pinton, Comprehensive analysis of mitochondrial permeability transition pore activity in living cells using fluorescence-imaging-based techniques, Nat. Protoc. 11 (2016) 1067–1080, https://doi.org/10.1038/nprot.2016.064.
[43] C. Algieri, C. Bernardini, F. Oppedisano, D. La Mantia, F. Trombetti, E. Palma, M. Forni, V. Mollace, G. Romeo, S. Nesci, Mitochondria bioenergetic functions and cell metabolism are modulated by the bergamot polyphenolic fraction, Cells 11 (2022) 1401, https://doi.org/10.3390/cells11091401.
[44] M. Forte, S. Marchitti, M. Cotugno, F. Di Nonno, R. Stanzione, F. Bianchi, L. Schirone, S. Schiavon, D. Vecchio, G. Sarto, M. Scioli, S. Raffa, G. Tocci, M. Relucenti, M.R. Torrisi, V. Valenti, F. Versaci, C. Vecchione, M. Volpe, G. Frati, S. Rubattu, S. Sciarretta, Trehalose, a natural disaccharide, reduces stroke occurrence in the stroke-prone spontaneously hypertensive rat, Pharmacol. Res. 173 (2021), 105875, https://doi.org/10.1016/j.phrs.2021.105875.
[45] J.R. Gledhill, M.G. Montgomery, A.G.W. Leslie, J.E. Walker, Mechanism of inhibition of bovine F1-ATPase by resveratrol and related polyphenols, Proc. Natl. Acad. Sci. U. S. A 104 (2007) 13632–13637, https://doi.org/10.1073/pnas.0706290104.
[46] G.L. Orriss, A.G. Leslie, K. Braig, J.E. Walker, Bovine F1-ATPase covalently inhibited with 4-chloro-7-nitrobenzofurazan: the structure provides further support for a rotary catalytic mechanism, Structure 6 (1998) 831–837.
[47] S. Di Castro, S. Scarpino, S. Marchitti, F. Bianchi, R. Stanzione, M. Cotugno, L. Sironi, P. Gelosa, E. Duranti, L. Ruco, M. Volpe, S. Rubattu, Differential modulation of uncoupling protein 2 in kidneys of stroke-prone spontaneously hypertensive rats under high-salt/low-potassium diet, Hypertension 61 (2013) 534–541, https://doi.org/10.1161/HYPERTENSIONAHA.111.00101.
[48] S. Rubattu, M. Volpe, R. Kreutz, U. Ganten, D. Ganten, K. Lindpaintner, Chromosomal mapping of quantitative trait loci contributing to stroke in a rat model of complex human disease, Nat. Genet 13 (1996) 429–434, https://doi.org/10.1038/ng0896-429.
[49] M. Volpe, G. Iaccarino, C. Vecchione, D. Rizzoni, R. Russo, S. Rubattu, G. Condorelli, U. Ganten, D. Ganten, B. Trimarco, K. Lindpaintner, Association and cosegregation of stroke with impaired endothelium-dependent vasorelaxation in stroke prone, spontaneously hypertensive rats, J. Clin. Invest 98 (1996) 256–261, https://doi.org/10.1172/JCI118787.
[50] S. Rubattu, S. Di Castro, H. Schulz, A.M. Geurts, M. Cotugno, F. Bianchi, H. Maatz, O. Hummel, S. Falak, R. Stanzione, S. Marchitti, S. Scarpino, B. Giusti, A. Kura, G. F. Gensini, F. Peyvandi, P.M. Mannucci, M. Rasura, S. Sciarretta, M.R. Dwinell, N. Hubner, M. Volpe, Ndufc2 gene inhibition is associated with mitochondrial dysfunction and increased stroke susceptibility in an animal model of complex human disease, J. Am. Heart Assoc. 5 (2016), https://doi.org/10.1161/JAHA.115.002701.
[51] T.M. Bauer, E. Murphy, Role of mitochondrial calcium and the permeability transition pore in regulating cell death, Circ. Res 126 (2020) 280–293, https://doi.org/10.1161/CIRCRESAHA.119.316306.
[52] M. Forte, L. Schirone, P. Ameri, C. Basso, D. Catalucci, J. Modica, C. Chimenti, L. Crotti, G. Frati, S. Rubattu, G.G. Schiattarella, D. Torella, C. Perrino, C. Indolfi, S. Sciarretta, Italian society of cardiology working group on cellular and molecular biology of the heart, the role of mitochondrial dynamics in cardiovascular diseases, Br. J. Pharmacol. 178 (2021) 2060–2076, https://doi.org/10.1111/bph.15068.
[53] V. Izzo, J.M. Bravo-San Pedro, V. Sica, G. Kroemer, L. Galluzzi, Mitochondrial permeability transition: new findings and persisting uncertainties, Trends Cell Biol. 26 (2016) 655–667, https://doi.org/10.1016/j.tcb.2016.04.006.
[54] P. Bernardi, F.Di Lisa, The mitochondrial permeability transition pore: molecular nature and role as a target in cardioprotection, J. Mol. Cell. Cardiol. 78 (2015) 100–106, https://doi.org/10.1016/j.yjmcc.2014.09.023.
[55] P. Bernardi, F. Di Lisa, F. Fogolari, G. Lippe, From ATP to PTP and back: a dual function for the mitochondrial ATP synthase, Circ. Res. 116 (2015) 1850–1862, https://doi.org/10.1161/CIRCRESAHA.115.306557.
[56] J. Karch, M.J. Bround, H. Khalil, M.A. Sargent, N. Latchman, N. Terada, P. M. Peixoto, J.D. Molkentin, Inhibition of mitochondrial permeability transition by deletion of the ANT family and CypD, Sci. Adv. 5 (2019) eaaw4597, https://doi.org/10.1126/sciadv.aaw4597.
[57] M.A. Neginskaya, M.E. Solesio, E.V. Berezhnaya, G.F. Amodeo, N. Mnatsakanyan, E.A. Jonas, E.V. Pavlov, ATP synthase C-subunit-deficient mitochondria have a small cyclosporine a-sensitive channel, but lack the permeability transition pore, e2, Cell Rep. 26 (2019) 11–17, https://doi.org/10.1016/j.celrep.2018.12.033.
[58] N. Mnatsakanyan, M.C. Llaguno, Y. Yang, Y. Yan, J. Weber, F.J. Sigworth, E. A. Jonas, A mitochondrial megachannel resides in monomeric F1FO ATP synthase, Nat. Commun. 10 (2019) 5823, https://doi.org/10.1038/s41467-019-13766-2.
[59] A. Urbani, V. Giorgio, A. Carrer, C. Franchin, G. Arrigoni, C. Jiko, K. Abe, S. Maeda, K. Shinzawa-Itoh, J.F.M. Bogers, D.G.G. McMillan, C. Gerle, I. Szabò, P. Bernardi, Purified F-ATP synthase forms a Ca2+-dependent high-conductance channel matching the mitochondrial permeability transition pore, Nat. Commun. 10 (2019) 4341, https://doi.org/10.1038/s41467-019-12331-1.
[60] K.N. Alavian, G. Beutner, E. Lazrove, S. Sacchetti, H.-A. Park, P. Licznerski, H. Li, P. Nabili, K. Hockensmith, M. Graham, G.A. Porter, E.A. Jonas, An uncoupling channel within the c-subunit ring of the F1FO ATP synthase is the mitochondrial permeability transition pore, Proc. Natl. Acad. Sci. U. S. A. 111 (2014) 10580–10585, https://doi.org/10.1073/pnas.1401591111.
[61] M. Bonora, A. Bononi, E. De Marchi, C. Giorgi, M. Lebiedzinska, S. Marchi, S. Patergnani, A. Rimessi, J.M. Suski, A. Wojtala, M.R. Wieckowski, G. Kroemer, L. Galluzzi, P. Pinton, Role of the c subunit of the FO ATP synthase in mitochondrial permeability transition, Cell Cycle 12 (2013) 674–683, https://doi.org/10.4161/cc.23599.
[62] G. Pinke, L. Zhou, L.A. Sazanov, Cryo-EM structure of the entire mammalian F-type ATP synthase, Nat. Struct. Mol. Biol. 27 (2020) 1077–1085, https://doi.org/10.1038/s41594-020-0503-8.
[63] S. Nesci, A. Pagliarani, C. Algieri, F. Trombetti, Mitochondrial F-type ATP synthase: multiple enzyme functions revealed by the membrane-embedded FO structure, Crit. Rev. Biochem. Mol. Biol. 55 (2020) 309–321, https://doi.org/10.1080/10409238.2020.1784084.
[64] S. Nesci, The mitochondrial permeability transition pore in cell death: a promising drug binding bioarchitecture, Med. Res. Rev. 40 (2020) 811–817, https://doi.org/10.1002/med.21635.
[65] A. Stocco, N. Smolina, P. Sabatelli, J. Šileikytė, E. Artusi, V. Mouly, M. Cohen, M. Forte, M. Schiavone, P. Bernardi, Treatment with a triazole inhibitor of the mitochondrial permeability transition pore fully corrects the pathology of sapje zebrafish lacking dystrophin, Pharmacol. Res. (2021), 105421, https://doi.org/10.1016/j.phrs.2021.105421.
[66] S. Nesci, C. Algieri, F. Trombetti, V. Ventrella, M. Fabbri, A. Pagliarani, Sulfide affects the mitochondrial respiration, the Ca2+-activated F1FO-ATPase activity and the permeability transition pore but does not change the Mg2+-activated F1FO-ATPase activity in swine heart mitochondria, Pharm. Res 166 (2021), 105495, https://doi.org/10.1016/j.phrs.2021.105495.

[67] S. Herold, Nitrotyrosine, dityrosine, and nitrotryptophan formation from metmyoglobin, hydrogen peroxide, and nitrite, Free Radic. Biol. Med. 36 (2004) 565–579, https://doi.org/10.1016/j.freeradbiomed.2003.10.014.
[68] C.C. Moser, T.A. Farid, S.E. Chobot, P.L. Dutton, Electron tunneling chains of mitochondria, Biochim. Biophys. Acta BBA Bioenerg. 2006 (1757) 1096–1109, https://doi.org/10.1016/j.bbabio.2006.04.015.
[69] D. Bald, T. Amano, E. Muneyuki, B. Pitard, J.L. Rigaud, J. Kruip, T. Hisabori, M. Yoshida, M. Shibata, ATP synthesis by F0F1-ATP synthase independent of noncatalytic nucleotide binding sites and insensitive to azide inhibition, J. Biol. Chem. 273 (1998) 865–870, https://doi.org/10.1074/jbc.273.2.865.
[70] L. Castro, V. Demicheli, V. Tórtora, R. Radi, Mitochondrial protein tyrosine nitration, Free Radic. Res. 45 (2011) 37–52, https://doi.org/10.3109/10715762.2010.516254.
[71] J. Wang, S. Toan, H. Zhou, New insights into the role of mitochondria in cardiac microvascular ischemia/reperfusion injury, Angiogenesis 23 (2020) 299–314, https://doi.org/10.1007/s10456-020-09720-2.
[72] E. Murphy, C. Steenbergen, Mechanisms underlying acute protection from cardiac ischemia-reperfusion injury, Physiol. Rev. 88 (2008) 581–609, https://doi.org/10.1152/physrev.00024.2007.
[73] S. Rubattu, R. Stanzione, M. Volpe, Mitochondrial dysfunction contributes to hypertensive target organ damage: lessons from an animal model of human disease, Oxid. Med. Cell Longev. 2016 (2016) 1067801, https://doi.org/10.1155/2016/1067801.
[74] B. Li, C. Chauvin, D. De Paulis, F. De Oliveira, A. Gharib, G. Vial, S. Lablanche, X. Leverve, P. Bernardi, M. Ovize, E. Fontaine, Inhibition of complex I regulates the mitochondrial permeability transition through a phosphate-sensitive inhibitory site masked by cyclophilin D, Biochim. Biophys. Acta 2012 (1817) 1628–1634, https://doi.org/10.1016/j.bbabio.2012.05.011.